The application of bifurcation theory to study the nonlinear dynamical phenomena in an electrical power system

by

Byongjun Lee

A Thesis Submitted to the

Graduate Faculty in Partial Fulfillment of the

Requirements for the Degree of

MASTER OF SCIENCE

Department: Electrical Engineering and Computer Engineering
Major: Electrical Engineering

Iowa State University
Ames, Iowa
1991

TABLE OF CONTENTS

LIST OF FIGURES

LIST OF TABLES

ACKNOWLEDGMENTS

I am deeply indebted to my major professor, Dr. Ajjarapu, for providing me with guidance and direction during my research work and in times of doubt. I would also like to extend my gratitude both to the Electric Power Research Center for providing me with financial assistance during my graduate program and to the members of the power faculty under whom I undertook my graduate courses.

Finally, I would like to thank my family members (my father and mother, my wife Eunjoo, and my brother and sisters) for their help and encouragement.

CHAPTER 1. INTRODUCTION

Current Situation

Because today's power systems are often heavily loaded and highly stressed, operating them is becoming increasingly difficult. Power system operating practices have evolved so that now the transmission network functions quite differently from the way it did a decade or so ago. It is not surprising that heretofore uncommon, even unheard–of, network–instability mechanisms have been linked to major power system failures in several countries. One such operational problems occurs in the area of system voltages, which gradually decrease as the system load increases. In some instances, voltage collapse has caused blackouts. The condition in which this collapse may occur is called the critical point, or the collapse point. Power systems may also evidence nonlinear oscillatory behavior resulting in an inter–area mode oscillation or parametric resonance phenomena [1, 2].

Necessity of Studying Nonlinearity

Voltage collapse or nonlinear oscillatory phenomena generally occur in stressed power systems. In stressed power systems, nonlinear effects are of great importance for capturing infrequent phenomena. Previous studies have either not included nonlinear model or have not considered one properly.

In general, solving or analyzing nonlinear dynamical equations is very difficult and requires special techniques. To avoid these difficulties, systems are generally linearized in an attempt to predict their behavior. These linearized equations, however, may not predict true system behavior. Recent advances in nonlinear dynamical system theory and in bifurcation theory have made it possible to analyze dynamical systems in a systematic way. These theories show how nonlinearity affects the behavior of a system. In this thesis, an attempt has been made to show the importance of nonlinearity in terms of its effect on the operation of a power system network.

Scope of This Work

Recently, nonlinear analysis has been undergoing important developments. In this thesis, our aim is to use the bifurcation theory to explain certain nonlinear phenomena. Bifurcation theory basically deals with the qualitative change of system state according to variations of an particular parameter of the system. This theory was applied to a sample power system network to study the effect of variations of one parameter on the behavior of the system. Systematic application of the theory revealed the existence of both stable and unstable periodic solutions as well as the conditions leading to voltage collapse. A particular response depends upon the value of the parameter under consideration. It was discovered that voltage collapse is a subset of overall bifurcation phenomena that a system may undergo when influenced by system parameters. A low dimensional center manifold reduction was applied to reveal the relevant dynamics involved in the voltage collapse process.

Literature Review

The literature on voltage collapse from dynamic considerations is extensive. The earlier work of Thomas and Tiranuchit considered the effect of load dynamics [3]. These investigations found that induction motor dynamics could affect voltage instability before a steady–state bifurcation point was reached. Dobson et al. [4] developed the voltage collapse model, which includes load as well as generator dynamics. In their study, the dynamics of the voltage collapse process were analyzed around the critical point.

Abed and Varaiya, on the other hand, examined the oscillatory behavior of the power system according to Hopf bifurcation theory [5]. Although the Hopf bifurcation point can be the critical point in a power system operation, it is qualitatively different from the conventional critical point. Alexander [6] and Rajagopalan et al. [7] also studied system instability around the Hopf bifurcation point.

In general, under the variation of a certain parameter, a dynamic system may become unstable in two ways, depending upon how the eigenvalues leave the left half of the complex plane. First, one or more real system eigenvalues may become positive, and, second, a pair of complex conjugate eigenvalues may cross the imaginary axis. The voltage collapse problem studied by Dobson et al. is related to the former way, for load voltage dominates system instability. On the other hand, [5, 6, 7] considered the latter way, which includes generator dynamics.

Ajjarapu and Lee studied two qualitatively different system instabilities due to bifurcation in a sample power system model [8, 9]. In their preliminary study, they raised the possibility of coexistence of 1) oscillatory type of instability and 2) voltage collapse depending upon the value of the parameter under consideration. They also

enumerated the conditions and parameter values necessary to obtain one of these phenomena.

This thesis, the extended version of work reported in [8] and [9], consists of two parts. The first part constitutes Chapters 2, 3, and 4, which introduce mathematical concepts necessary to understand the work reported. In Chapter 2, the principles of bifurcation phenomena and the determination of dynamical system stability are broadly discussed. In Chapter 3, bifurcation theory is reviewed. Real and complex bifurcations are defined, and the bifurcation diagram is used to show various branching behaviors. In Chapter 4, the stability of the stationary or the periodic branch is discussed. The monodromy matrix and the Floquet multiplier are introduced as tools to analyze the stability of the periodic branch. Application of the above mathematical concepts to a sample power system network is discussed in the second part of the thesis, which consists of Chapters 5 and 6. Chapter 5 deals exclusively with the analysis of oscillatory phenomena, whereas Chapter 6 concentrates on the dynamics involved in the voltage collapse process.

CHAPTER 2. CONCEPTS OF BIFURCATION AND LINEAR STABILITY

Everyday, we experience gradual or sudden changes. Consider the following simple experiment discussed in reference [10]. Imagine a board somehow supported at both ends and load (p) on top of it. If load p is small enough, the board will be bent with the deformation depending upon the weight of load p and the physical properties of the board (such as its stiffness). This state of the board will remain stable; that is a small variation in the load (or in the stiffness) will lead to a slightly perturbed state. Such a variation would be referred to as a quantitative change. The board is deformed within its elastic regime and will return to its original shape when the perturbation is removed.

Nevertheless, the situation changes abruptly when the load is increased beyond a certain critical level, p_0, upon which the board breaks. This sudden event is an example of a qualitative change. Suppose the shape of the board is modeled by some function (solution of an equation). We, thus, might say that there exists a solution for load values $p < p_0$, and that this solution ceases to exist for $p > p_0$. Load p and stiffness are examples of parameters, which control the outcome of any experiment or of any event. Varying a parameter can result in a transition from a quantitative change to a qualitative change. The following pairs of verbs may serve as illustrations:

bend → break

stretch → tear

inflate → burst

The verbs on the left side stand for states that are stable under small perturbation; the response of each system is a quantitative one. The related drastic and irreversible change is reflected by the verbs on the right side.

The abovementioned problems are much too limited to cover phenomena that we will later refer to with the term bifurcation. The extended range of phenomena we have in mind is indicated by the pair

stationary state → motion.

Transition from a stationary state to motion, and vice versa, is a qualitative change. Here, again, in terms of solutions – of governing equations – we have a different quality of solution on either side of a critical parameter. Let the parameter in question again be denoted by p, with the critical value being p_0. In terms of wind speed, for instances, the state (for example, of a flag) is stationary for $p < p_0$ and oscillatory for $p > p_0$. Qualitative changes may come in several steps, as indicated by the sequence [10]

stationary state,

regular motion,

irregular motion.

The transition from regular to irregular motion is related to the onset of turbulence, or chaos. As a first tentative definition, we will refer to a qualitative change caused by the variation of some physical parameter p, such as branching or bifurcation.

Some important features that may change at bifurcations have already been mentioned. The following list summarizes various kinds of qualitative changes as mentioned in [10]:

stable $\rightarrow$ unstable

symmetric $\rightarrow$ asymmetric

stationary $\rightarrow$ periodic (regular) motion

regular $\rightarrow$ irregular

order $\rightarrow$ chaos

Several of these changes may take place simultaneously and in complicated ways. A thorough discussion of such branching phenomena will be undertaken in terms of bifurcation theory. Before proceeding to the mathematical analysis of stability and bifurcation, we shall review a number of important principles in the remaining sections.

Fundamentals of Stationary Points and Their Stability

Suppose the state of a two variable system is described by functions $f_1(t)$ and $f_2(t)$:

$$\dot{y}_1 = f_1(y_1, y_2), \tag{2.1}$$

$$\dot{y}_2 = f_2(y_1, y_2). \tag{2.2}$$

Equilibrium points (y_1^s, y_2^s) are defined by $\dot{y}_1 = 0$ and $\dot{y}_2 = 0$. At the equilibrium points, the system is at rest. The points y_1^s, y_2^s are also called stationary points. Stationary points are solutions of the system of equations given by the right-hand side of the following differential equations:

$$f_1(y_1^s, y_2^s) = 0, \tag{2.3}$$

$$f_2(y_1^s, y_2^s) = 0. \tag{2.4}$$

The stability of stationary points is defined as follows:

> The stationary solution y^s is said to be stable if the response to a small perturbation remains small as the time approaches infinity. Otherwise, the stationary point is called unstable or nonstable.

Stability can be determined from the eigenvalue analysis as follows. Let us take a Taylor series expansion of f_1 and f_2 about (y_1^s, y_2^s).

$$\begin{aligned}
\dot{y}_1 &= f_1(y_1, y_2) \\
&= f_1(y_1^s, y_2^s) + \frac{\partial f_1}{\partial y_1}(y_1^s, y_2^s)(y_1 - y_1^s) + \frac{\partial f_1}{\partial y_2}(y_1^s, y_2^s)(y_2 - y_2^s) \cdots, \\
\dot{y}_2 &= f_2(y_1, y_2) \\
&= f_2(y_1^s, y_2^s) + \frac{\partial f_2}{\partial y_1}(y_1^s, y_2^s)(y_1 - y_1^s) + \frac{\partial f_2}{\partial y_2}(y_1^s, y_2^s)(y_2 - y_2^s) \cdots.
\end{aligned}$$

Because $f_1(y_1^s, y_2^s) = f_2(y_1^s, y_2^s) = 0$, dropping the second and higher order terms yields two differential equations linear in $y_1 - y_1^s$ and in $y_2 - y_2^s$. This system of equations can subsequently be expressed by

$$\dot{y} = J_s y, \tag{2.5}$$

where

$$y = \begin{pmatrix} y_1 \\ y_2 \end{pmatrix},$$

$$J_s = \begin{pmatrix} \frac{\partial f_1}{\partial y_1}(y_1^s, y_2^s) & \frac{\partial f_1}{\partial y_2}(y_1^s, y_2^s) \\ \frac{\partial f_2}{\partial y_1}(y_1^s, y_2^s) & \frac{\partial f_2}{\partial y_2}(y_1^s, y_2^s) \end{pmatrix}.$$

Clearly, the eigenvalues λ_1 and λ_2 of the Jacobian are the roots of the characteristic equation

$$det(J_s - \lambda I) = 0,$$

where I is the identity matrix. The linear approximation of $y_1(t)$ and $y_2(t)$ is formulated as follows:

$$y_1(t) - y_1^s = c_1\eta_1 e^{\lambda_1 t} + c_2\eta_2 e^{\lambda_2 t}, \tag{2.6}$$

$$y_2(t) - y_2^s = c_3\eta_3 e^{\lambda_1 t} + c_4\eta_4 e^{\lambda_2 t}, \tag{2.7}$$

where $c_i, i = 1, \cdots, 4$, are scalar constants corresponding to the initial value. $(\eta_1, \eta_3)^T$ and $(\eta_2, \eta_4)^T$ are the eigenvectors corresponding to eigenvalues λ_1 and λ_2, respectively, which is denoted by the vector notation $\lambda = (\lambda_1, \lambda_2)$ in this thesis. The real part of eigenvalues gives the rate of expansion (if $Re[\lambda_i] > 0$) or contraction (if $Re[\lambda_i] < 0$) in the neighborhood of the equilibrium point along the direction of η_i.

If $Re[\lambda_i] < 0$ for all λ_i, then for all sufficiently small perturbations, the stationary point is stable. If some $Re[\lambda_i] > 0$, then the stationary point is not stable and is either unstable (all $Re[\lambda_i] > 0$) or nonstable (one of $Re[\lambda_i] < 0$ and the other $Re[\lambda_i] > 0$). When the stationary point is nonstable, it needs further analysis. Stability at the nonstable stationary points depends upon the direction of the perturbation.

Depending upon the type of eigenvalues, three cases can be obtained:

Case 1: λ_1, λ_2 Real, $\lambda_1\lambda_2 > 0$, $\lambda_1 \neq \lambda_2$

In this case, when both eigenvalues are real and have the same sign, the stationary point is called the node. There are, moreover, two subcases:

- $\lambda < 0$ implies that $\lim_{t\to\infty} e^{\lambda t} = 0$. Therefore, $y(t)$ converges to y^s in a sufficiently small neighborhood of the node. This type, in which perturbations die out, is called a stable node.

- $\lambda > 0$ implies that $\lim_{t\to\infty} e^{\lambda t} = \infty$. As a consequence, $y(t)$ diverges locally; that is, the trajectories $y(t)$ leave the neighborhood of the node, which is hence unstable.

Case 2: λ_1, λ_2 Real, $\lambda_1\lambda_2 < 0$

When the real eigenvalues have different signs, the stationary point is called the saddle point. Under this condition, the solution $y(t)$ has a stable solution if the perturbation is in the direction of the eigenvector associated with the negative eigenvalue. Otherwise, the solution is always unstable.

Case 3: λ_1, λ_2 Complex Conjugate With Nonzero Real Part

Let $\lambda_1 = \alpha + j\beta$ and $\lambda_2 = \alpha - j\beta$, where α and $\pm\beta$ denote real and imaginary parts, respectively. The time-dependent part of $y(t)$ is thus

$$e^{(\alpha\pm j\beta)t} = e^{\alpha t} e^{\pm j\beta t}.$$

The phase $e^{\pm j\beta t} = \cos\beta t \pm j \sin\beta t$ represents rotation, (counterclockwise if $\beta > 0$; and clockwise if $\beta < 0$). The phase $e^{\alpha t}$ has a radius of increasing value if $\alpha > 0$

and a radius of decreasing value if $\alpha < 0$. In time, β indicates frequency, and α the amplitude of an oscillating wave. The corresponding equilibrium is therefore called either an unstable ($\alpha > 0$) or a stable ($\alpha < 0$) focus.

When the $y(t)$ has a stable solution, the steady-state solution is called a point attractor. The next section will introduce an attractor that is qualitatively different from a steady-state attractor.

Fundamentals of Limit Cycles

As emphasized earlier, stability and instability results are of a local nature. Even if one is able to find all the equilibria of a particular problem, putting all the local pieces together is not guaranteed to give a complete, global picture. There are other attractors not so easy to obtain as equilibria. One such attractor is the limit cycle. A limit cycle represents regular motions. Examples are voltage or currents in electrical circuits and vibrations of violin strings in air.

Consider the Van der Pol equation, a differential equation of the second order, in which nonlinearity results from damping:

$$\ddot{u} - \lambda(1 - u^2)\dot{u} + u = 0. \tag{2.8}$$

The second-order Van der Pol equation (Equation 2.8) can be transformed into two first-order differential equations by means of, for instance, $y_1 = u, y_2 = \dot{u}$:

$$\begin{aligned} \dot{y}_1 &= y_2, \\ \dot{y}_2 &= \lambda(1 - y_1^2)y_2 - y_1. \end{aligned}$$

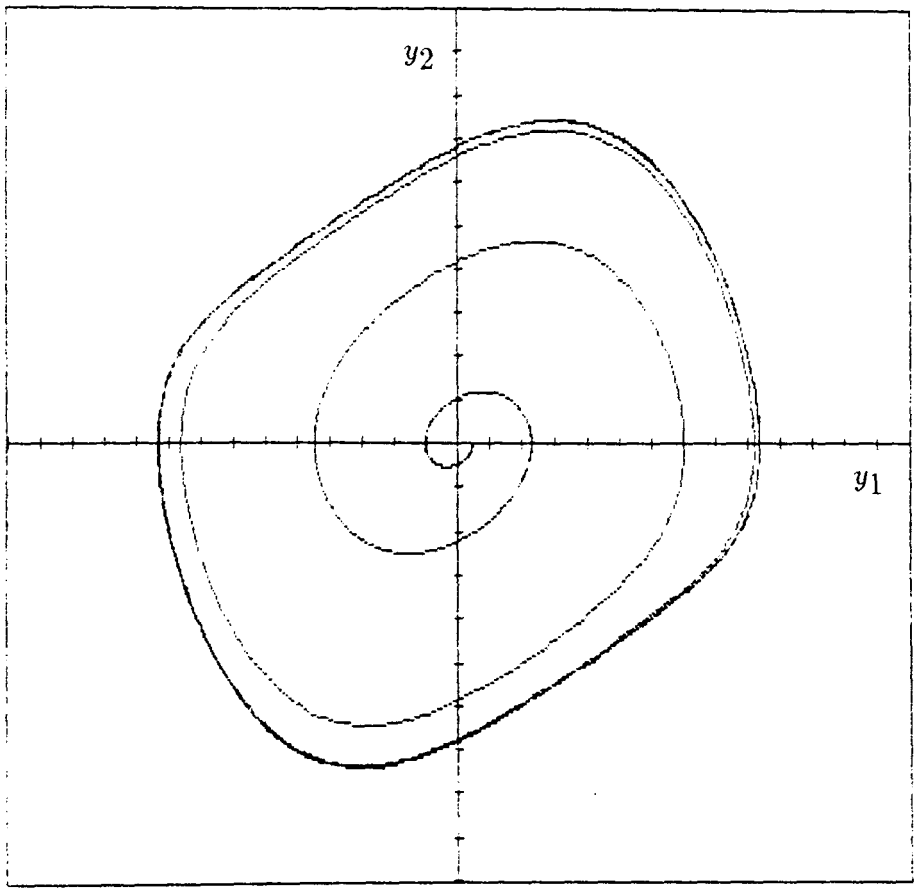

Figure 2.1: The trajectory of the limit cycle for initial value $(y_1, y_2) = (0.0, 0.1)$

This system has one stationary solution at $(y_1^s, y_2^s) = (0,0)$. For $0 < \lambda < 2$, this point is unstable [10]. To discuss the dynamics of the system for small positive values of λ, a numerical time simulation is applied for the finite time intervals $0 \leq t \leq t_f$. The trajectory for the data

$$y_1(0) = 0.1, \quad y_2(0) = 0.0, \quad t_f = 50.0, \quad \lambda = 0.5$$

is plotted in Figure 2.1, where it can be seen that the trajectory approaches a closed curve and remains there. Such a closed curve towards which the trajectory winds is termed a *limit cycle*. A limit cycle is a periodic solution (orbit); i.e., after some period T, the solution values will be the same:

$$y(t+T) = y(t). \tag{2.9}$$

Trajectories starting outside the limit cycle also wind towards it. Limit cycles are stable if they are approached by nearby trajectories. Orbits are unstable when trajectories leave their neighborhoods. The Van der Pol equation has a stable limit cycle for $0 < \lambda < 2$.

Additional Remarks

In the preceding sections, the basic principles of branching phenomena and of linear stability were clarified. The next chapter discusses various bifurcation phenomena and how the center manifold can be used to analyze nonlinear dynamical systems.

CHAPTER 3. REVIEW OF BIFURCATION THEORY

Introduction

Bifurcation theory has become a major focus of research in the analysis of nonlinear dynamical systems. Central to this topic is the question of whether the qualitative properties of a dynamical system change with the variation of certain of its parameters. Generally, if certain of the parameters of any physical or natural system continue to vary, a critical stage may be reached in which the system makes a sudden jump from one state to another. The new state may be qualitatively, and sometimes quantitatively, different from the original state.

Change of state is described in terms of the eigenvalue of the dynamical system. If the parameter is varied slowly, the eigenvalues of the Jacobian evaluated on the solution path change accordingly. As mentioned in the previous chapter, if the real part of eigenvalues moves to the right hand side of the imaginary axis in eigenspaces, the system can reach a critical state.

The travelling of eigenvalues from one half plane to another can be realized in one of two qualitatively different ways. Generally, when real eigenvalues cross the imaginary axis, new branches of stationary solutions arise. If a pair of complex conjugate eigenvalues cross the imaginary axis, then there is a possibility of a periodic branch. Other cases are possible, but this study will be confined to the cases where

one real eigenvalue becomes zero, or a pair of complex conjugate eigenvalues are purely imaginary.

Autonomous Dynamical System

Consider a power system dynamical model described by autonomous differential equations of the vector form in n–dimensional space,

$$\dot{\mathbf{x}} = \mathbf{F}(\mathbf{x}, p), \tag{3.1}$$

where

$$\mathbf{x} = (x_1, x_2, \cdots, x_n)^T,$$

$$\mathbf{F} = (f_1, f_2, \cdots, f_n)^T.$$

Here, x_i denotes the state variable (generator angle, generator angular velocity, load voltage magnitude or angle, etc.), p is a time invariant scalar parameter (real or reactive power, etc.), and $\dot{\mathbf{x}}$ denotes $\frac{dx}{dt}$ where t is time.

The system is autonomous; i.e., the time variable does not appear explicitly in the right hand side of the Equation 3.1. We assume that the right hand side is continuous and continuously differentiable. Because the vector field does not depend upon time, the initial time may always be taken at $t_0 = 0$. The solution is called the trajectory and is denoted by $x(t, x_0)$. The dynamical system 3.1 is linear if $f_i(x)$ is.

Bifurcations in an Autonomous Dynamical System

Near an equilibrium point, the left–hand side term $\dot{x}$ of Equation 3.1 becomes zero; i.e., the steady–state (stationary) solution $\mathbf{x}$ of 3.1 satisfies the set of nonlinear

algebraic equations:

$$\mathbf{F}(\mathbf{x}, \mathbf{p}) = 0. \tag{3.2}$$

As stated in Chapter 2, the stability of the stationary solution x for a given p is determined by the eigenvalues of the linearized system, i.e., by the eigenvalues of the Jacobian matrix $\mathbf{J} = [\partial f_i / \partial x_j]$ evaluated for this stationary solution. The elements of the Jacobian matrix $\mathbf{J}$ continuously depend upon p (with continuous dependence of the stationary solution $x(p)$). Hence, the eigenvalues of J also continuously depend upon p. When, with the variation of the parameter, one or more eigenvalues cross the imaginary axis, the stability of the stationary solution can change. Let p_0 be the critical value of a parameter for which the real part of one or more eigenvalues becomes zero. For $p < p_0$ all the eigenvalues of J are in the complex left-half plane. Subsequently, the stationary solution satisfies the following conditions in the sense of local analysis:

- $p < p_0$, it is stable.
- $p = p_0$, it is critical.
- $p < p_0$, it is either unstable or nonstable.

At (x^*, p_0), if the eigenvalue is equal to zero, it follows from the implicit function theorem that the equilibria of 3.1 for value p different from p_0 can be expressed as the smooth function $x = x(p)$. The function $x(p)$ is called a branch of equilibria. If at (x^*, p_0), several branches of equilibria come together, the point (x^*, p_0) is said to be a bifurcation point. In Figure 3.1, solid and dashed lines depict branches of equilibrium. The solid lines represent stable equilibrium, and the dashed line unstable equilibrium. As can be seen from the bifurcation diagram, a formerly single

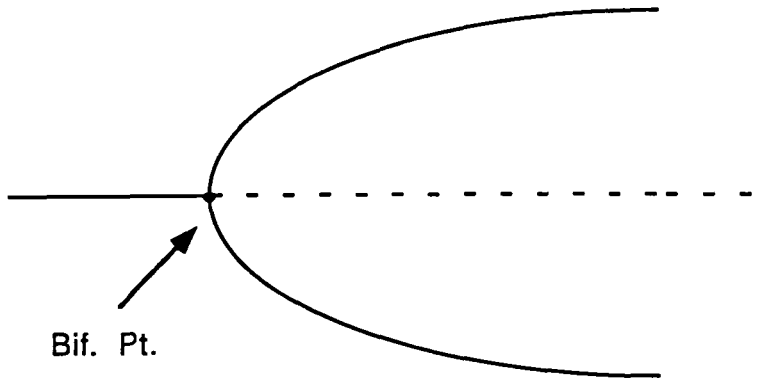

Figure 3.1: A bifurcation diagram

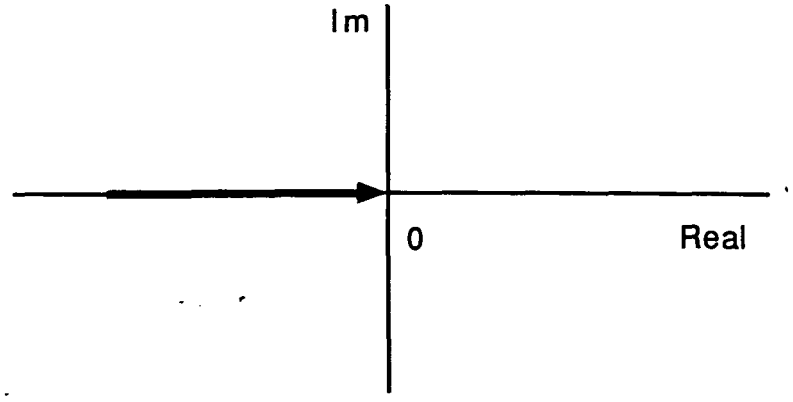

Figure 3.2: Real bifurcation

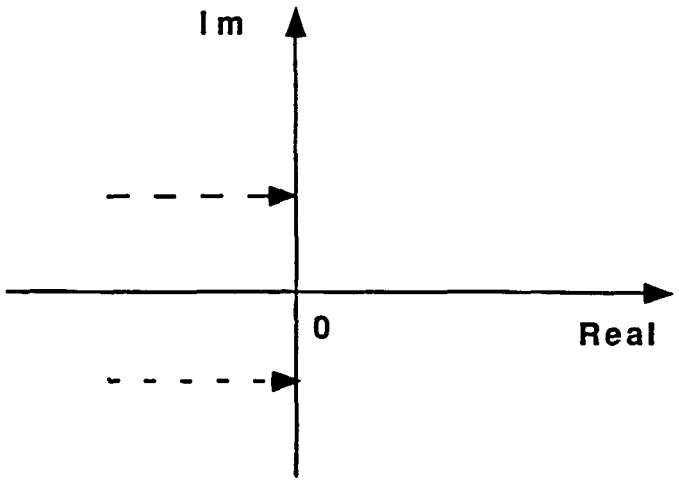

Figure 3.3: Complex bifurcation

equilibrium bifurcates into several distinct equilibria at the bifurcation point. The value of p at which the bifurcation occurs is called the bifurcation point.

As mentioned in the introduction to this chapter, we will discuss the instances in which 1) a real eigenvalue becomes zero and 2) a pair of complex conjugate eigenvalues are purely imaginary. In the former case, new branches of stationary solutions usually arise, called real bifurcation. The latter instance may lead to the arising of a branch of periodic solutions called complex bifurcation.

Real Bifurcations

Let us consider the case in which the real eigenvalue crosses the imaginary axis. We shall assume that the function f_i has first and second derivatives. The classi-

fication of point (x^*, p) satisfying 3.1 will be discussed in the following subsections [10].

Fold Bifurcation

The simple example of fold bifurcation can be introduced by the one-dimensional system

$$\dot{y} = y^2 \pm \lambda, \tag{3.3}$$

where $y \in R$, and $\lambda \in R$.

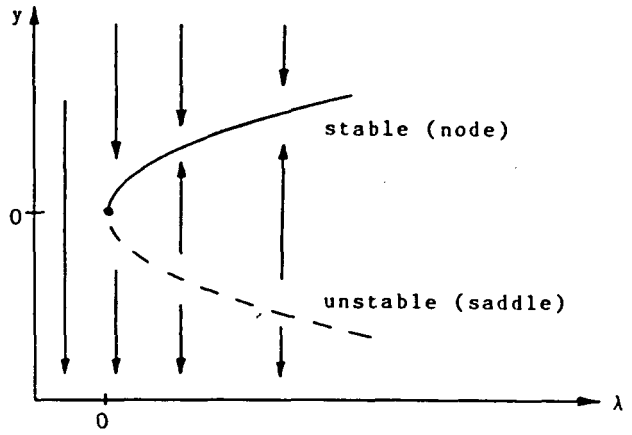

Figure 3.4: Fold bifurcation diagram

Figure 3.4 illustrates the bifurcation diagram of the equation $\dot{y} = y^2 - \lambda$. The equilibria $y(\lambda)$ of $y^2 - \lambda = 0$ form a parabola defined only for $\lambda \geq 0$. For $\lambda = 0$, there is only one solution ($y = 0$), whereas for $\lambda > 0$ there are two equilibria: $y = \sqrt{\lambda}$, and $y = -\sqrt{\lambda}$. The point at which solutions begin to exist ($\lambda = 0$, and $y = 0$ in this example) is a peak. The branch in Figure 3.4 comes from one side and turns back

at the turning point (emphasized by the dot in Figure 3.4). This point is called the turning or limit point or the saddle node.

The phrase saddle node implies the stable behavior of the solutions when regarded as equilibria of differential equations. Clearly, the equilibrium $\sqrt{\lambda}$ is stable, whereas $-\sqrt{\lambda}$ is not. The stable branch is called the node and the unstable branch the saddle. The bifurcation diagram of equation $\dot{y} = y^2 + \lambda$ presents a picture symmetrical with respect to $\lambda = 0$.

In summary, locally there are no solutions on one side of a turning point, but there are two solutions on the other side. At a turning point, two solutions either are born or extinguish each other.

Transcritical Bifurcation

Fold bifurcation implies that no equilibrium exists for parameter values smaller for $\dot{y} = y^2 - \lambda$ or larger for $\dot{y} = y^2 + \lambda$ than the bifurcation value. A dynamical system can have at least one equilibrium for any parameter value regarding the exchange of stability of a persisting equilibrium; a case in point is transcritical bifurcation, which is characterized by an exchange of stability of the origin. Figure 3.5 represents a transcritical bifurcation diagram for the equation

$$\dot{y} = \lambda y - y^2. \tag{3.4}$$

The solutions are $y = 0$ and $y = \lambda$. Stable branches are indicated by solid lines. For $\lambda < \lambda_0 = 0$, the origin $y = 0$ is the only stable equilibrium point. If $\lambda > \lambda_0$, then the equilibrium $y = 0$ becomes unstable, and a new stable equilibrium line emerges. The bifurcation diagram of the equation $\dot{y} = -\lambda y - y^2$ is symmetrical with respect to $\lambda = 0$.

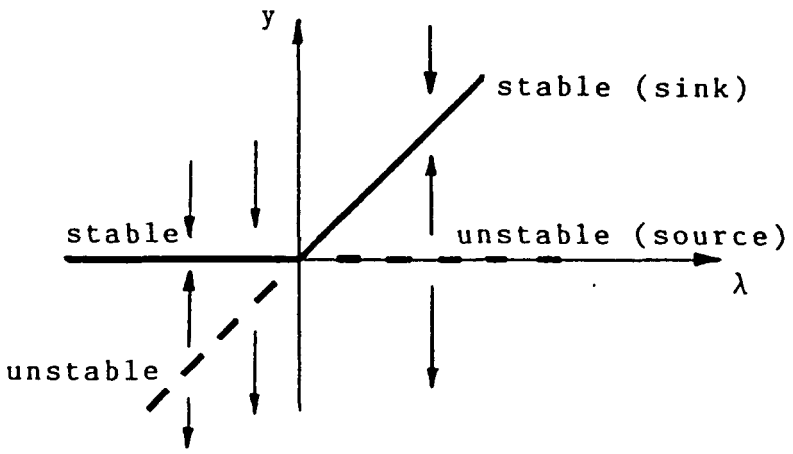

Figure 3.5: Transcritical bifurcation diagram

Pitchfork Bifurcation

A final example of the bifurcation of an equilibrium into two or more stable and unstable equilibria occurs with so-called pitchfork bifurcation. This type of bifurcation can occur in dynamical systems of 3.1 although the assumption is made that f_i is an odd function with respect to x.

Figure 3.6 shows the bifurcation diagram for the equation

$$\dot{y} = \lambda y - y^3. \tag{3.5}$$

For $\lambda > 0$, there are two nontrivial equilibria, $y = \pm\sqrt{\lambda}$. The transition of stability is shown in Figure 3.6. For $\lambda < \lambda_0 = 0$, the origin $y = 0$ is the only stable equilibrium point. When $\lambda > \lambda_0$, however, the equilibrium $y = 0$ becomes unstable, and two new stable branches emerge. This type of bifurcation is called supercritical bifurcation.

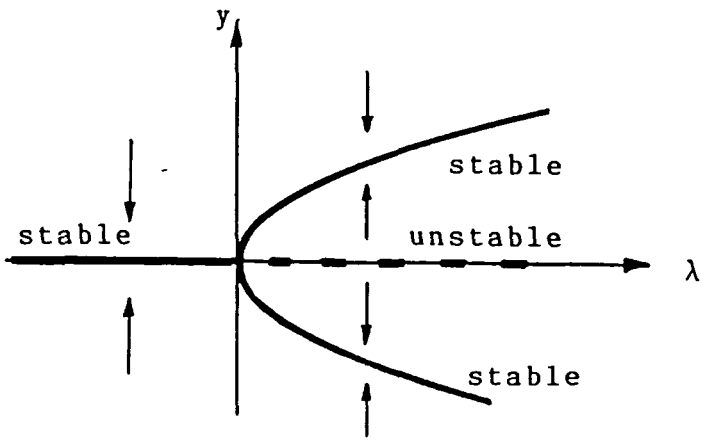

Figure 3.6: Supercritical pitchfork bifurcation diagram

Let us consider another equation:

$$\dot{y} = \lambda y + y^3, \tag{3.6}$$

Whose bifurcation diagram appears in Figure 3.7. There is a loss of stability at the bifurcation point $(y, \lambda) = (0, 0)$. In contrast to Figure 3.6, however, there is no exchange of stability. Instead, stability is lost locally at the bifurcation point. This type of bifurcation is called subcritical bifurcation. So far, we have considered only the simplest examples of one-dimensional systems. Because the dimension of dynamical systems considered in a practical situation is quite high, analyzing these systems is not always so simple. Nonetheless, it may be possible to reduce the high dimensional manifold to the low dimensional center manifold, thereby characterizing the relevant dynamics near critical points. The next section explains this reduction technique.

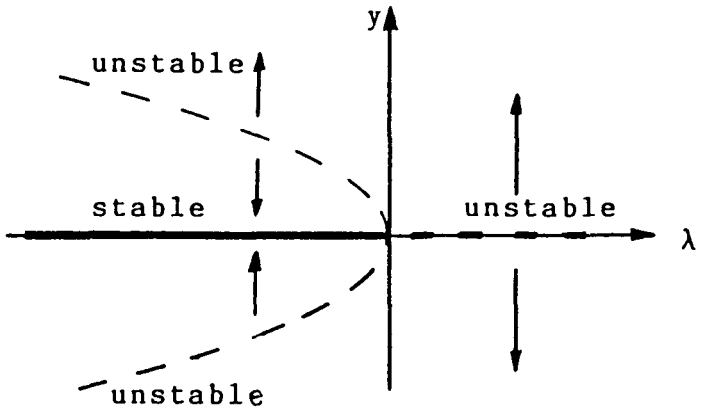

Figure 3.7: Subcritical pitchfork bifurcation diagram

Center Manifold Reduction

In this section, we will introduce the center manifold–reduction technique, which is usually used in the investigation of bifurcations and of the stability of bifurcated solutions. The basic concepts of the center manifold theory will be described briefly.

The solution structure of the linear system

$$\dot{\mathbf{x}} = A\mathbf{x} \tag{3.7}$$

is characterized by the eigenvalues and by the corresponding eigenspaces of matrix A. Each of the eigenspaces is invariant. The term invariant is defined as follows:

> Let a set S be a subset of R^n, and for any initial value, let x_0 be contained in S. If we have $x(t, 0, x_0)$, which is contained in f for all t, then the set

S is said to be invariant under the vector field $\dot{x} = f(x)$.

Eigenspaces are examples of invariant sets. Therefore, the solutions with initial conditions on the eigenspaces remain in that space. In nonlinear system 3.1, which posseses a fixed point at x^*, although invariant subspaces are retained, they are no longer linear (flat) spaces; they become curved. We thus have smooth invariant manifolds composed of solution curves. One may, however, have other fixed points or limit cycles in a nonlinear system, and thus this description is generally useful only locally; i.e., near x^*.

It is convenient to separate the locally decaying solutions from the growing ones. Thus, we define stable, unstable, and center eigenspaces E^s, E^u, and E^c of the matrix A as those spaces spanned by eigenvectors belonging to eigenvalues of A with negative, positive, and zero real parts, respectively. Orbits starting in E^s decay to zero as $t \to \infty$; orbits starting in E^u become unbounded as $t \to \infty$, and orbits starting in E^c neither grow nor decay exponentially as $t \to \infty$, depending upon the nonlinear terms. In the nonlinear case, however, we have invariantly stable, unstable, and center manifolds W^s, W^u, and W^c, which are tangent to E^s, E^u, and E^c at x^*.

If the system has only stable and center eigenspaces, then the flow is restricted to E^c. Long term behavior is dominated by the center manifold, which can be obtained as follows:

Consider the n–dimensional system given by 3.1. As p varies, let l eigenvalues cross the imaginary axis simultaneously with other $n-l$ eigenvalues remaining in the left half plane. The center manifold theorem implies that there is a local nonlinear change of the coordinates

$$\Psi : x \to y \quad or \quad y = \Psi(x), \tag{3.8}$$

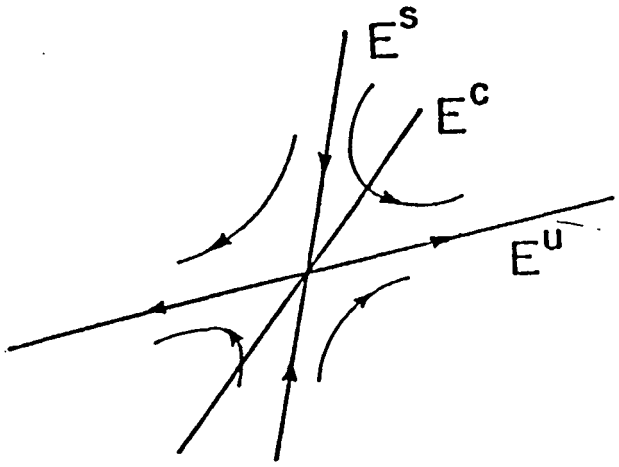

Figure 3.8: Eigenspaces

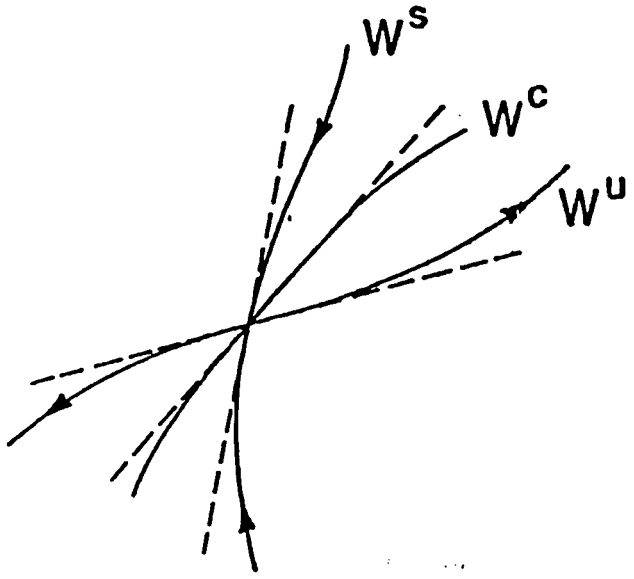

Figure 3.9: Invariant manifolds

such that in y coordinates, Eq 3.1 can be studied in the form

$$\begin{pmatrix} \dot{y_c} \\ \dot{y_s} \end{pmatrix} = \begin{pmatrix} B & 0 \\ 0 & C \end{pmatrix} \begin{pmatrix} y_c \\ y_s \end{pmatrix} + \begin{pmatrix} G_1(y_c, y_s, p) \\ G_2(y_c, y_s, p) \end{pmatrix}, \tag{3.9}$$

where all the eigenvalues of B have zero real parts, and all the eigenvalues of C have negative real parts. We assume that the coordinates of y have been chosen in such a way that the origin is an equilibrium point and that G_1, G_2 are strictly nonlinear. In Eq. 3.9, y_s is a stable manifold because its behavior is dominated by the C eigenvalues having negative real parts. At the origin, G_1 and G_2 vanish along with their first derivatives. The loss of stability is determined by the variables y_c. The stable manifold can be expressed locally as a function of y_c:

$$y_s = h(y_c), \tag{3.10}$$

and if we incorporate Eq. 3.10 into Eq.3.9, then

$$\begin{pmatrix} \dot{y_c} \\ \dot{y_s} \end{pmatrix} = \begin{pmatrix} B & 0 \\ 0 & C \end{pmatrix} \begin{pmatrix} y_c \\ h(y_c) \end{pmatrix} + \begin{pmatrix} G_1(y_c, h(y_c), p) \\ G_2(y_c, h(y_c), p) \end{pmatrix}, \tag{3.11}$$

where $h(0) = \dot{h}(0) = 0$, which implies that W^c is tangent to E^c at x^*. Although the function of $h(y_c)$ may be obtained by directly solving Eq. 3.9 in the form of functional differential equations, in general, it is very difficult to do so. The polynomial of Taylor expansion can be used to approximate the closed form of Eq. 3.10:

$$h(y_c) = a_1 y_c^2 + a_2 y_c^3 + \cdots. \tag{3.12}$$

Differentiating Eq. 3.10 with respect to time implies that the $\dot{y_s}, \dot{y_c}$ coordinates of any point on W^c must satisfy

$$\dot{y_s} = Dh(y_c)\dot{y_c}, \tag{3.13}$$

where D denotes $\frac{d}{dy_c}$. All points on W^c obey the dynamics generated by Eq. 3.9. Therefore, replacing $\dot{y}_s$ and $\dot{y}_c$ in Eq. 3.13 with Eq. 3.11 and at the same time incorporating the y_s of Eq. 3.10 into Eq. 3.13 gives

$$Dh(y_c)[By_c + G_1(y_c, h(y_c))] = Ch(y_c) + G_2(y_c, h(y_c), p), \tag{3.14}$$

or

$$Dh(y_c)[By_c + G_1(y_c, h(y_c))] - Ch(y_c) + G_2(y_c, h(y_c), p) = 0. \tag{3.15}$$

Therefore, to find a center manifold, all we need to do is to solve Eq. 3.15. Let us observe Eq. 3.13 carefully. If we assume that only one real eigenvalue becomes zero, i.e., $l = 1$, then, because $B = 0$ and G_1 is strictly nonlinear, $\dot{y}_c$ is expanded into

$$\dot{y}_c = d_1 y_c^2 + d_2 y_c^3 + \cdots. \tag{3.16}$$

$h(y_c)$ of Eq. 3.12 consists of terms with orders greater than two. Therefore, when $h(y_c)$ is substituted with y_s in Eq. 3.13, the coefficients of a_i are involved in terms of an order greater than or equal to cubic term. Therefore, the coefficient d_1 is not multiplied by a_i and d_1 can be obtained directly, without solving Eq. 3.15. In this work, the steps involved in calculations up to Eq. 3.15 are made using the symbolic package *MACSYMA* [11].

Hopf Bifurcation

In this section, we shall discuss the instance in which a pair of complex conjugate eigenvalues becomes zero. Under certain circumstances, a branch of periodic solutions (limit cycles) arises adjacent to the branch of stationary solutions. In short, a fixed point is bifurcated into a closed orbit in a neighborhood of the equilibrium.

The type of bifurcation that connecting equilibria with periodic motion is commonly referred to as Hopf Bifurcation [10] (because it was E. Hopf who proved the following theorem for the n–dimensional case in 1942).

Let us assume

1. $F(x_C, p_C) = 0$;
2. The Jacobian matrix $[\partial F/\partial x]$ has a simple pair of purely imaginary eigenvalues $\mu(p_C) = \pm i\omega_0$; and
3. $d(Re(\mu(p_C)))/dp \neq 0$.

There is subsequently a birth or death of limit cycles at (x_C, p_C), depending upon the sign of the derivative in 3.

The value p_C is the Hopf bifurcation value. Requirement 3 guarantees that there is a transversal crossing of the imaginary axis by the pair of complex conjugate eigenvalues. The Hopf bifurcation concludes more specifically that a one-parameter family of periodic solutions $x(t, \epsilon)$ of Eq. 3.1 always exists in the neighborhood of (x_C, p_C). If the derivative in 3 is positive, then the conjugate pair of eigenvalues moves into the right half plane. The parameter ϵ can be chosen so that

$$x = x_C + \epsilon x_1(t) + \cdots \tag{3.17}$$

$$p = p_C + p_2\epsilon^2 + \cdots \tag{3.18}$$

$$T = 2\pi/\omega_0 + T_2\epsilon^2 + \cdots \tag{3.19}$$

in which $T = T(\epsilon)$ is the period of $x(t, \epsilon)$ [12]. In particular, $x(t, \epsilon) \to x_0, p(\epsilon) \to p_0, T(\epsilon) \to 2\pi/\omega_0$ as $\epsilon \to 0^+$. Furthermore, the stability of the periodic solution $x(t, \epsilon)$ can be determined as follows.

In the above mentioned instance, periodic solutions have the Floquet exponent $\beta(\epsilon) = \beta_2\epsilon^2 + \cdots$, where $\beta_2 = -2p_2 dRe(\mu(p_c))/dp_c$ [8,9]. The stability of the periodic branch emanating from the stationary branch is determined by β_2. Periodic solutions exist either supercritically or subcritically if β_2 is negative or positive, respectively. When the bifurcation is supercritical, the periodic branch is initially stable, and when subcritical, initially unstable [12].

Example of Hopf Bifurcation

Let us consider the Lorenz equations for a sample system [13] motivated by the problem of weather forecasting:

$$\dot{x}_1 = 10(-x_1 + x_2) \tag{3.20}$$

$$\dot{x}_2 = -x_1 x_3 + r x_1 - x_2 \tag{3.21}$$

$$\dot{x}_3 = x_1 x_2 - 2.666 x_3 \tag{3.22}$$

where x_i is the real variable, and r the parameter. $\dot{x}_i$ denotes dx/dt, where t is dimensionless time.

We solve the algebraic equations by putting zero to the left hand side. It reveals the certain facts, namely, there are three solutions depending only on r, thus:

- zero solution

$$x_{1s} = 0$$

$$x_{2s} = 0$$

$$x_{3s} = 0$$

- upper solution

$$\begin{aligned} x_{1s} &= \sqrt{2.666(r-1)} \\ x_{2s} &= \sqrt{2.666(r-1)} \\ x_{3s} &= r-1 \end{aligned}$$

- lower solution

$$\begin{aligned} x_{1s} &= -\sqrt{2.666(r-1)} \\ x_{2s} &= -\sqrt{2.666(r-1)} \\ x_{3s} &= r-1. \end{aligned}$$

Nonzero solutions appear for $r \geq 1$. The bifurcation diagram for the Lorenz equations takes the form shown in Figs. 3.10, 3.11, and 3.12. The stability of each branch is easily assessed by studying the eigenvalues of the Jacobian matrix

$$J(x_s) = \begin{pmatrix} -10 & 10 & 0 \\ -x_{3s}+r & -1 & -x_{1s} \\ x_{2s} & x_{1s} & -2.666 \end{pmatrix}.$$

For the zero solution of this equastion, the eigenvalues are

$$\begin{aligned} \lambda_1 &= -2.666 \\ \lambda_2 &= 0.5(-11-\sqrt{81+40r}) \\ \lambda_3 &= 0.5(-11+\sqrt{81+40r}), \end{aligned}$$

where λ_1 and λ_2 are always negative and real. The eigenvalue λ_3 is always real, but for $r = 1$, it becomes zero, which is the supercritical pitchfork–bifurcation point (see

Figs. 3.10, 3.11, and 3.12). For values of r greater than one, zero solution branch becomes unstable, and the parabolic curve branches off at $r = 1$.

Along the upper branch, the characteristic equation for eigenvalues is

$$\lambda^3 + 13.666\lambda^2 + (r + 10)\lambda + 26.666(r - 1) = 0. \tag{3.23}$$

If we apply the Routh criterion to Eq. 3.23, we find one negative real eigenvalue and two complex eigenvalues along the upper branch. Complex eigenvalues have a negative real part up to $r_c = 23.734$ and a positive real part thereafter. The r_c is the critical value of r for the instability of parabolic branches. Finally, we can say that

- $0 < r < 1 \rightarrow$ no parabolic branch,
- $1 < r < r_c \rightarrow$ stable parabolic branches, and
- $r > r_c \rightarrow$ no steady-state stable solutions.

To investigate what happens in the neighborhood of r_c, let us apply the Hopf bifurcation theorem. We know that r_c is a critical solution; i.e., the real part of complex conjugate eigenvalues becomes zero. The transversality condition is

$$\frac{dRe\lambda(r_c)}{dr} = 3.051 > 0. \tag{3.24}$$

That is, with the increasing of r through the value of r_c, the real part of λ goes from negative to positive.

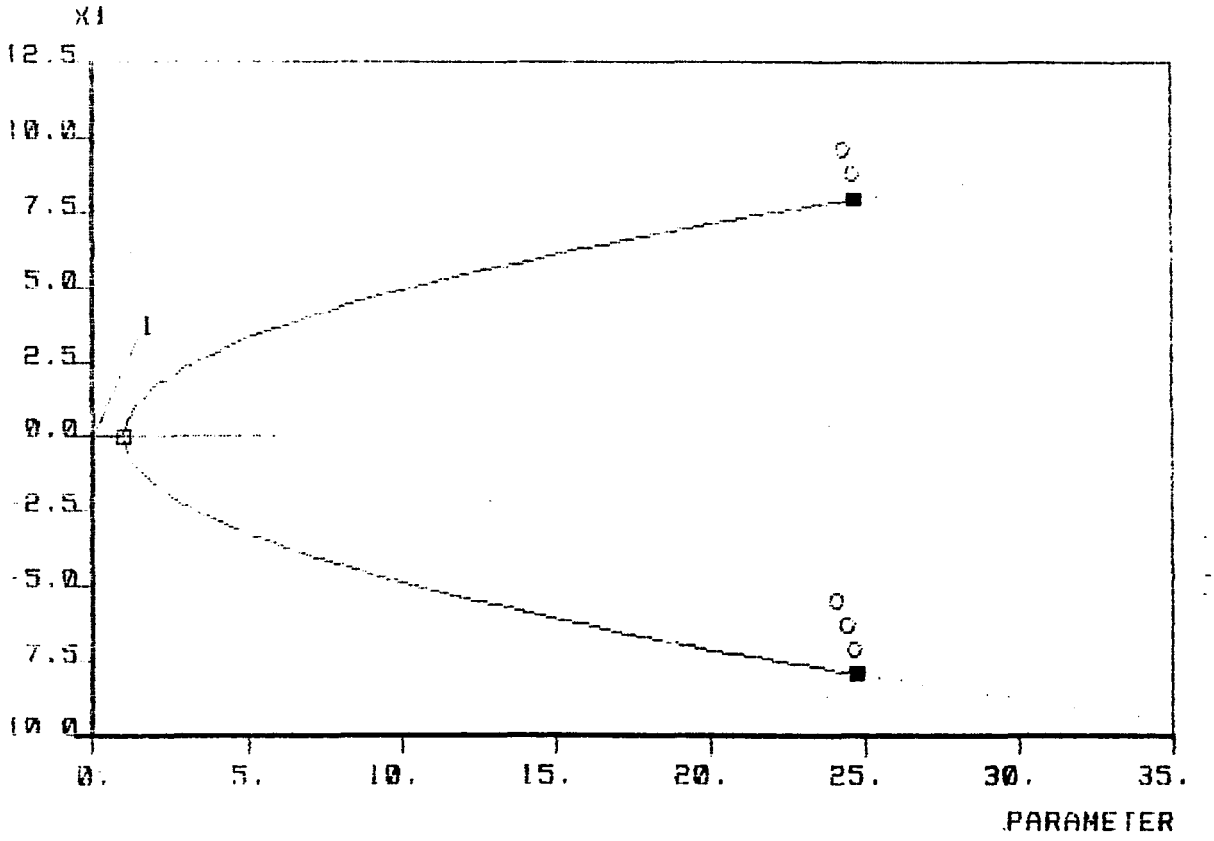

Figure 3.10: Bifurcation diagram: x_1 versus r of the Lorenz equation

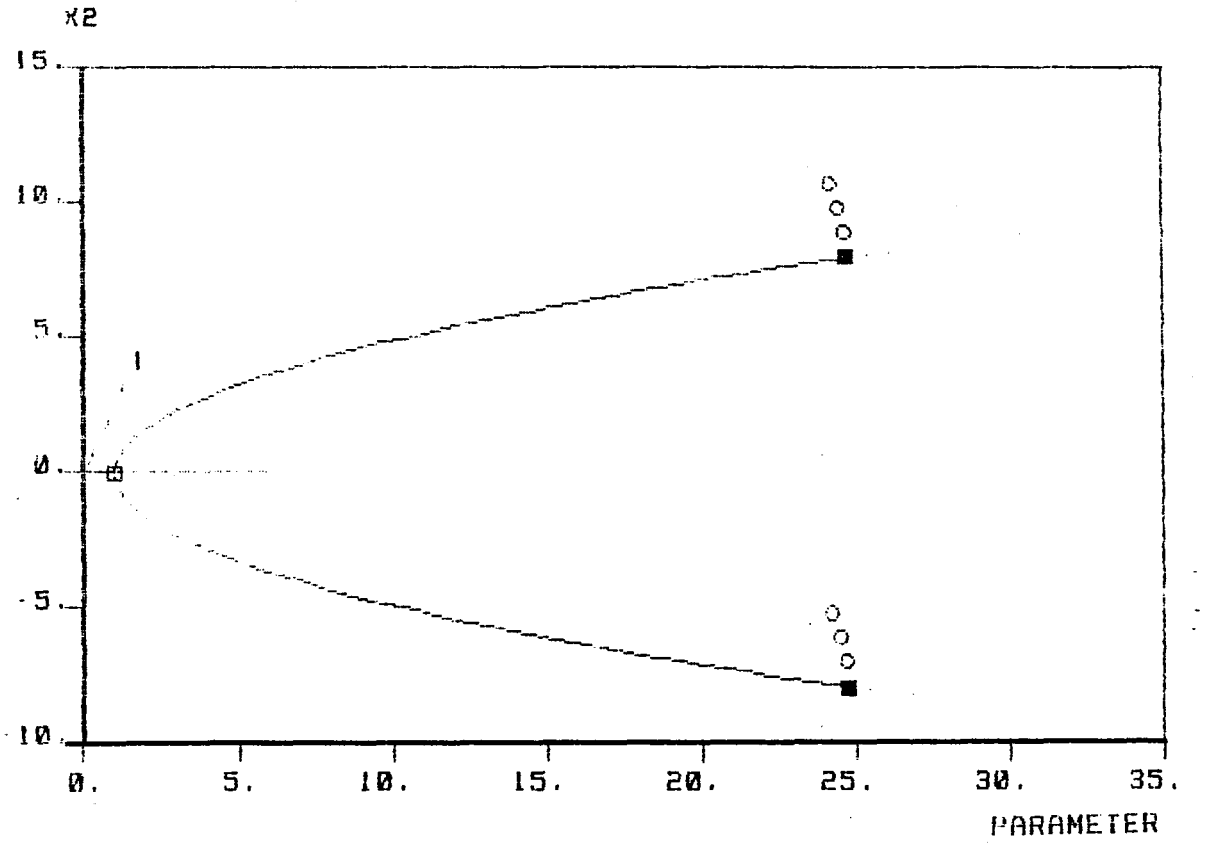

Figure 3.11: Bifurcation diagram: x_2 versus r of the Lorenz equation

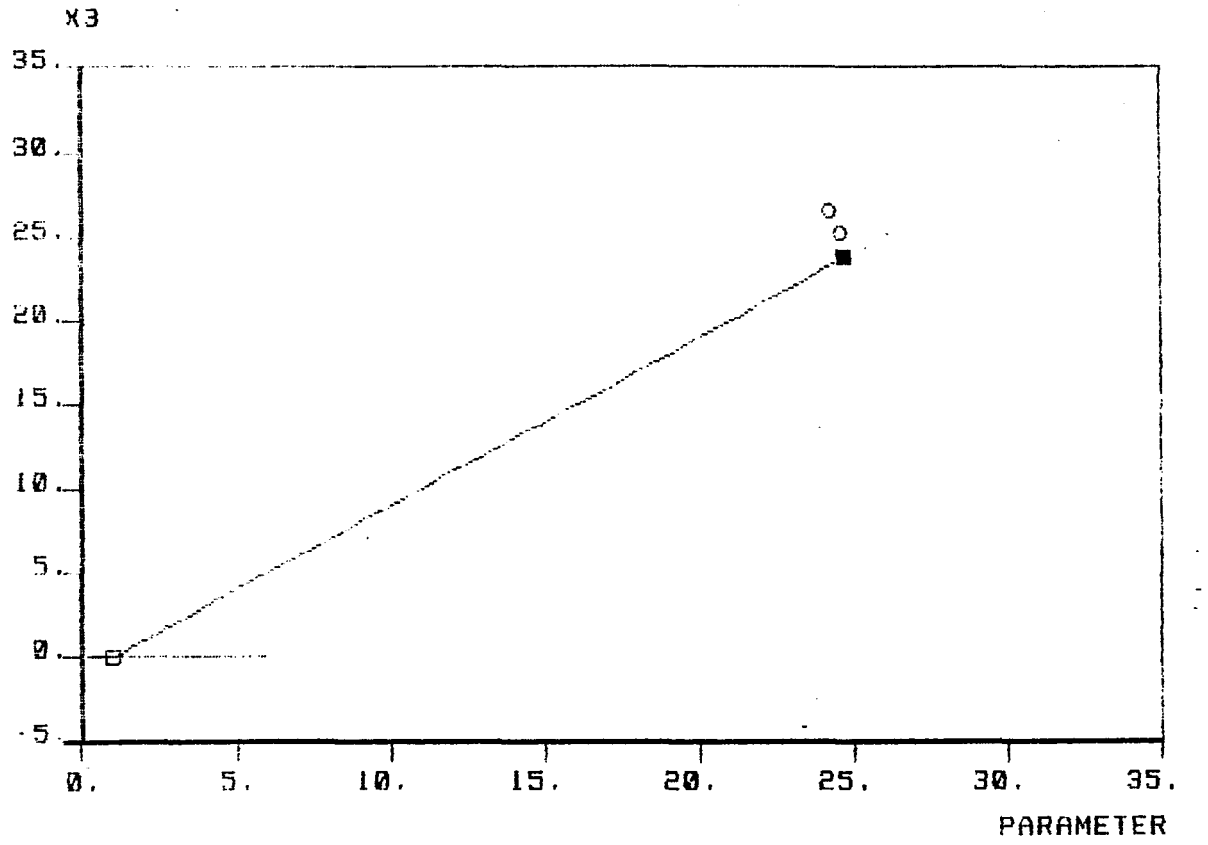

Figure 3.12: Bifurcation diagram: x_3 versus r of the Lorenz equation

Further Analysis Needed

In the previous section, the periodic orbit was discussed, and the conditions needed to obtain the periodic orbit were cited. The analyzing technique introduced in this chapter focuses on static analysis more or less. When we tackle the problem related to periodic motion, the eigenvalue analysis can no longer be adapted, and it becomes necessary to find a pertinent tool for further analysis of periodicity. In the next chapter, Floquet theory is employed to analyze system behavior on the periodic orbit. This theory plays a major role in the analysis of periodic motion, as does the eigenvalue analysis in the steady state.

CHAPTER 4. ANALYSIS OF PERIODIC SOLUTIONS

Introduction

In the previous chapter, we showed that a Hopf bifurcation point connects stationary solutions to periodic ones and guarantees the existence of a local periodic orbit emanating from the Hopf bifurcation point. With fixed parameters, the Hopf bifurcation theory provides the condition necessary to determine the local stability of this periodic orbit. Once the periodic orbit is established, the next step is to vary the parameter to trace the periodic branch. When a branch of periodic solutions is traced, questions arise as to: 1) whether the periodic solutions are stable, and 2) where and in what way stability is lost. In this chapter, a tool will be introduced to analyze the periodic solutions and their stability. Bifurcations on the periodic orbit, with the parameter variation, will be described, and the chapter concluded by introducing the possibility of chaotic behavior.

Monodromy Matrix

The existence of periodic orbit is guaranteed locally near the Hopf bifurcation point. The next step is to trace the periodic orbit as the parameter value increases. Each time the parameter is increased, the stability condition is investigated locally. Thus, the system state along the whole periodic orbit can be determined.

Consider solution x^* with period T along the periodic branch. The stability of periodic solutions can be studied in the framework of the method developed by Seydel [10] and Guckenheimer [14]. Trajectories of the differential equation can be defined by $x = \varphi(t, z)$, which is the periodic solution of Eq. 3.1 with z as an initial value; i.e., $\varphi(t+T, z) = \varphi(t, z)$. When Eq. 3.1 is perturbed with $z^* + d_0$, a trajectory progresses to the periodic orbit $x^* = \varphi(t, z^*)$ with the distance

$$d(t) = \varphi(t, z^* + d_0) - \varphi(t, z^*), \tag{4.1}$$

where z^* means the particular initial value for a particular solution. After one period T, the distance is measured by

$$d(T) = \varphi(T, z^* + d_0) - \varphi(T, z^*), \tag{4.2}$$

and its linear approximation with Taylor expansion becomes

$$d(T) = \frac{\partial \varphi(T, z^*)}{\partial z} d_0. \tag{4.3}$$

In Eq. 4.3, the matrix

$$\frac{\partial \varphi(T, z^*)}{\partial z} \tag{4.4}$$

governs the growth or decay of the initial perturbation d_0. The matrix in Eq. 4.4 is called a Monodromy matrix, and the eigenvalues of the monodromy matrix are called Floquet multipliers or characteristic multipliers [15].

Because $\varphi(t, z)$ is the solution of Eq.3.1, x can be replaced with $\varphi(t, z)$. Thus,

$$d\varphi(t, z)/dt = F(\varphi(t, z), p) \tag{4.5}$$

for all t. If we differentiate Eq. 4.5 with respect to z and use the chain rule,

$$\frac{d}{dt}\frac{\partial \varphi(t, z)}{\partial z} = \frac{\partial F(\varphi(t, z), p)}{\partial \varphi(t, z)}\frac{\partial \varphi(t, z)}{\partial z}. \tag{4.6}$$

If we assume that

$$\Phi(t) = \frac{\partial \varphi(t,z)}{\partial z}, \tag{4.7}$$

then Eq. 4.6 will be represented by the matrix equation, which solves the matrix initial value problem

$$\dot{\Phi}(t) = F_x(x,p)\Phi(t), \qquad \Phi(0) = z^*, \tag{4.8}$$

where $F_x(x,p)$ is the Jacobian of Eq. 3.1. Consequently the monodromy matrix corresponds to $\Phi(t)$ at t $= T$. To calculate the monodromy matrix, we integrate Eq. 4.8 for $0 \leq t \leq T$. Because $F_x(x,p)\Phi$ varies with $x(t)$, the Jacobian matrix should be provided for each t. One way to provide the Jacobian for all t's is to combine Eqs. 3.1 and 4.8 as an initial value problem.

$$\begin{pmatrix} \dot{x} \\ \dot{\Phi} \end{pmatrix} = \begin{pmatrix} F(x,p) \\ F_x(x,p)\Phi \end{pmatrix}, \qquad \begin{pmatrix} x(0) \\ \Phi(0) \end{pmatrix} = \begin{pmatrix} x^*(0) \\ z^* \end{pmatrix}$$

Then the periodic solution of Eq. 3.1, i.e., $x(t) = \varphi(t, x(0))$, is provided to evaluate the Jacobian matrix at each time step. Finally, when we integrate the initial value problem until $t = T$, then the monodromy matrix is given by $\Phi(T)$. To apply this method, a normalization has to be introduced to fix period T. Generally, the normalizing boundary condition

$$\dot{\Phi}(0) = \sum_{i=1}^{n} \frac{\partial F_x(x,p)}{\partial x_i}\Phi(0) = 0 \tag{4.9}$$

can be imposed. For simplicity, the integration interval will be normalized to $0 \leq t \leq 1$. After normalization, linearization takes the form

$$\dot{\Phi} = TF_x(x,p)\Phi, \;\; \Phi(0) = \Phi(1), \dot{\Phi}(0) = 0. \tag{4.10}$$

The periodic system thus has the boundary-value problem of dimension $2n + 2$:

$$\begin{pmatrix} \dot{x} \\ \dot{p} \\ \dot{T} \\ \dot{\Phi} \end{pmatrix} = \begin{pmatrix} TF(x,p) \\ 0 \\ 0 \\ TF_x(x,p)\Phi \end{pmatrix}$$

$$\begin{pmatrix} x(0) - x(1) \\ \Phi(0) - \Phi(1) \\ \sum_{i=1}^{n} \frac{\partial F_x(x(0),p)}{\partial x_i}\Phi(0) \\ \Phi(0) - 1 \end{pmatrix} = 0$$

Solving the above boundary value problem yields the periodic solution and the monodromy matrix.

The Floquet multipliers provide a useful tool for investigating the stability of periodic solutions. In the next section, we will show how to determine the stability of periodic solutions.

Stability of Periodic Solutions

Consider a periodic solution $x^*(t)$ on the periodic branch. The stability of the periodic solution is determined by linearizing f_i at $x^*(T)$. The linear system

$$\delta\dot{x}(t) = M(p)\delta x(t) \tag{4.11}$$

governs the local behavior of f_i near $x^*(T)$. The orbit of the system for initial condition $x^*(T) + \delta x_0$ is

$$f(x^*(T) + \delta x_0) \;=\; x^*(T) + \delta x(t) \tag{4.12}$$

$$
\begin{aligned}
&= x^*(T) + M(p)^t \delta x_0 \\
&= x^*(T) + c_1 \eta_1 \mu_1^t + \cdots + c_n \eta_n \mu_n^t,
\end{aligned}
$$

where $\mu_i, (i = 1, \cdots, n)$, and $\eta_i, (i = 1, \cdots, n)$ are the eigenvalues and eigenvectors of the monodromy matrix $M(p)$, and where $c_i, (i = 1, \cdots, n)$ are scalar constants chosen to achieve the correct initial condition.

The eigenvalues μ_i of monodromy matrix $M(p)$ are called the Floquet multipliers, or the characteristic multipliers, of periodic solution $x^*(t)$ at $t = T$, and they determine the amount of contraction($\mid \mu \mid < 1$) and expansion ($\mid \mu \mid > 1$) near $x^*(t)$ in the direction of η_i. To preserve periodicity, one of these n–Floquet multipliers is always equal to 1. The other $n - 1$ Floquet multiplier determines (local) stability.

- If all Floquet multipliers μ_i lie within the unit circle, then the periodic solution is asymptotically stable.

- If all Floquet multipliers μ_i lie outside the unit circle, then the periodic solution is unstable.

- If some Floquet multipliers lie within the unit circle and others lie outside it, then the periodic solution is nonstable. The stability of the periodic solution in such a case depends upon the direction of perturbation.

If one of the Floquet multipliers lies on the unit circle, then the stability of the periodic solution cannot be determined by these multipliers alone.

Bifurcation of Periodic Solutions

On the stable periodic orbit, $n-1$ Floquet multipliers are always inside the unit circle. Floquet multipliers are the function of the parameter under consideration; when we vary the parameters, the Floquet multipliers also change, and some of them may cross the unit circle. In this section, we shall discuss the stability of the periodic solutions in terms of variation of the parameter.

The stability of periodic solutions on one branch may change with variation of the system parameter because some of the Floquet multipliers may move outside of the unit circle in the complex plane. The Floquet multiplier crossing the unit circle is called the critical multiplier. Different types of branching occur depending upon where a critical multiplier, or a pair of complex conjugate multipliers cross the unit circle. Three associated types of branching are shown in Fig. 4.1. This figure shows the path of the critical multiplier only–i.e., the Floquet multiplier with $\mid \mu(p_C) \mid = 1$. In Fig. 4.1.a, the critical multiplier goes outside the unit circle along the positive real axis with $\mu(p_C) = 1$. In Fig. 4.1.b, the critical multiplier goes outside the unit circle along the negative real axis with $\mu(p_C) = -1$. In Fig. 4.1.c, a pair of complex conjugate multipliers cross the unit circle with a nonzero imaginary part. All three sketches refer to a loss of stability when p passes through p_C on one branch. On the other hand, changing the arrows to point in the reverse direction illustrates a gain of stability–i.e., a critical multiplier enters the unit circle.

If one multiplier passes through the unique circle at -1 on the real axis, the originally stable periodic solution becomes unstable, and a branch of periodic solutions with a doubled period branches off. The new branch can be either supercritical (branching of stable periodic solutions with period two) or subcritical (branching of

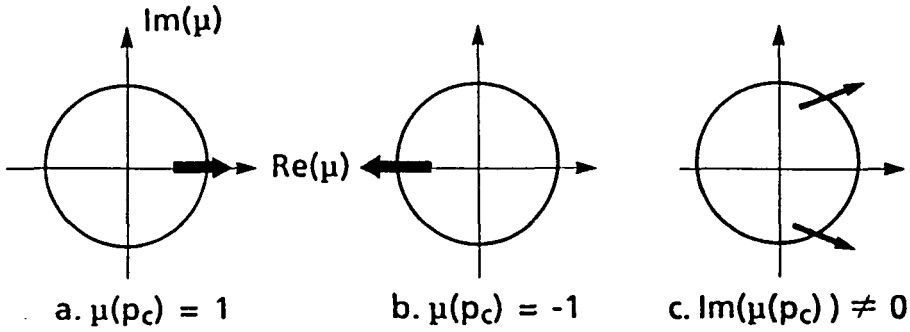

Figure 4.1: Three ways of losing stability

unstable periodic solutions with period two). The bifurcation, in which a Floquet multiplier intersects the unit circle through -1 is called the period-doubling bifurcation. The period-doubling bifurcation often multiplies its period and may lead to a more complex bifurcation called chaos, which will be discussed in the next section.

When the multiplier intersects the unit circle through $+1$, a limit point appears along the curve of the periodic solutions on a parameter space. This point may correspond to intermitency, in which periodic oscillations are alternated by active and passive dynamics in the neighborhood of that point [10]. When a pair of complex conjugate Floquet multipliers intersects the unit circle, the originally stable branch of the periodic solutions becomes unstable, and a stable or unstable torus may appear at the bifurcation point.

Chaotic Behavior

The oscillations we have discussed so far have been periodic. Periodicity reflects a high degree of regularity and order. Frequently, however, one encounters irregular oscillations that are either random or chaotic. The former are generally caused by the random disturbance or random variation of parameter, whereas the latter, although seemingly random, are generally caused by a deterministic equation without any evident random input or random variation of parameter. In this section we shall briefly discuss the characteristics of chaos.

Chaos can be characterized by two elements: geometrical features and sensitivity to initial conditions. Geometrical features are explained by tracing the trajectory in either the phase plane or the time domain. Trajectories are bounded but not periodic. They do not have the characteristic of uniform distribution. Another property of a chaotic system is sensitive dependence on initial conditions: given two different initial conditions arbitrarily close, the trajectories emanating from these points diverge at a rate characteristic of the system until they are uncorrelated. In practice, the initial state of a system can never be specified exactly, but only to within the tolerance $\varepsilon > 0$; if the two initial conditions x_0 and $\hat{x}_0$ lie within ε of one another, they cannot be distinguished. After a finite amount of time, however, $\phi_t(x_0)$ and $\phi_t(\hat{x}_0)$ will diverge and become unrelated. Therefore, no matter how precisely the initial condition is known, the longterm behavior of a chaotic system can never be predicted. This unpredictability can be considered the deterministics of random behavior. Figures. 4.2 and 4.3 show two characteristics of chaos for the Lorenz equations. Fig. 4.2 shows the chaotic trajectory in time plot. The waves are bounded but not periodic. The sensitive dependence on initial conditions is captured

in Figure 4.3. The initial values of the upper diagram and the lower diagram are 5.0 and 5.01, respectively. They differ by just 0.3 percent.

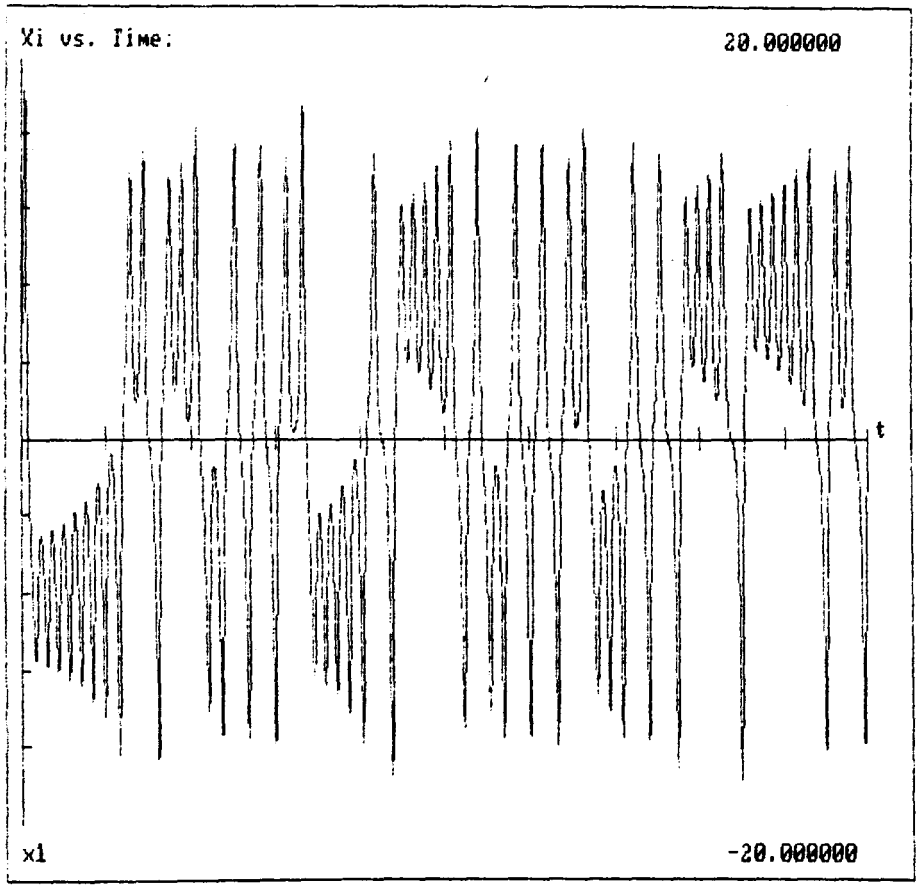

Figure 4.2: Chaotic trajectory of the first component of the Lorenz equation

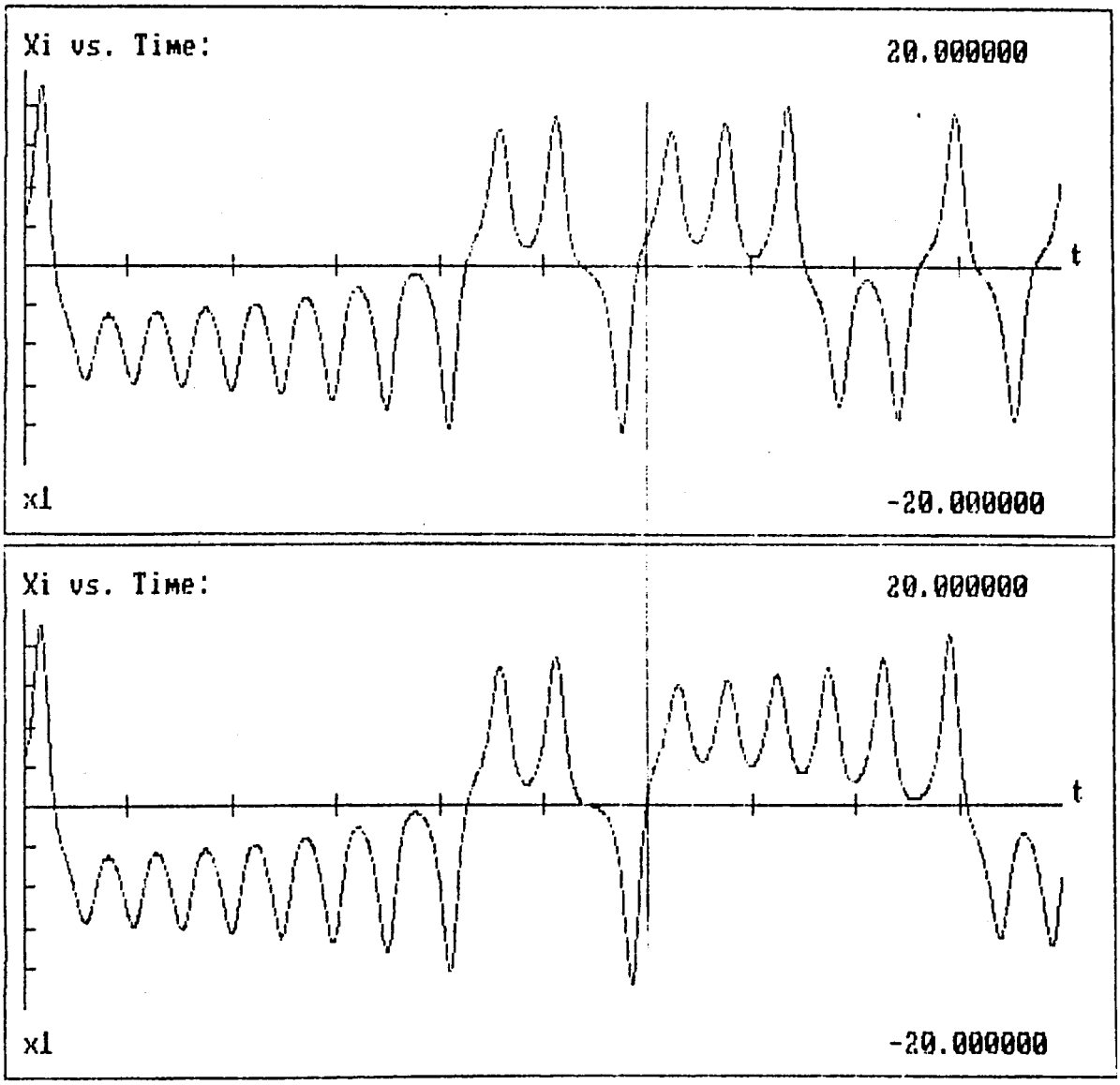

Figure 4.3: Two trajectories plotted versus time showing sensitive dependence on initial conditions in the Lorenz equation

Period–doubling Route to Chaos

In the previous section, we briefly discussed the characteristics of chaos. Because we are considering parameter–dependent equations, it is only natural to ask how chaos depends upon the system parameter p. We are particularly interested in how chaos arises, and for which values of the system parameter p one may expect chaotic behavior. Generally, there is no unique way in which chaos arises. In this section, we suggest a period–doubling route, that leads to chaos.

Let us consider the one–dimensional, discrete–time system

$$x_{t+1} = px_t(1 - x_t), \quad x_t \in [0, 1], \quad , p \in [0, 4], \tag{4.13}$$

which is the so–called logistic equation [13]. Without any analytic investigation, this example shows that the way to chaos is through a series of period–doubling bifurcations. Although this example is by far simpler than the actual systems, it serves well to illustrate the process of chaos. This simple example helps us to concentrate on concepts without becoming engulfed in details.

We assume $x_0 = 0.4$ for an initial value at $t = 0.0$. If we perform iterations for a particular $p = 2.0$,

$$\begin{aligned} x_1 &= px_0(1 - x_0) \\ x_2 &= px_1(1 - x_1) \\ &= p^2 x_0(1 - x_0)(1 - px_0(1 - x_0)), \\ &\vdots \end{aligned}$$

then the iterated value converges to the fixed value 0.5. If we increase p step by step, however, then the iterated value converges to a nonfixed value. At $p = 3.4$,

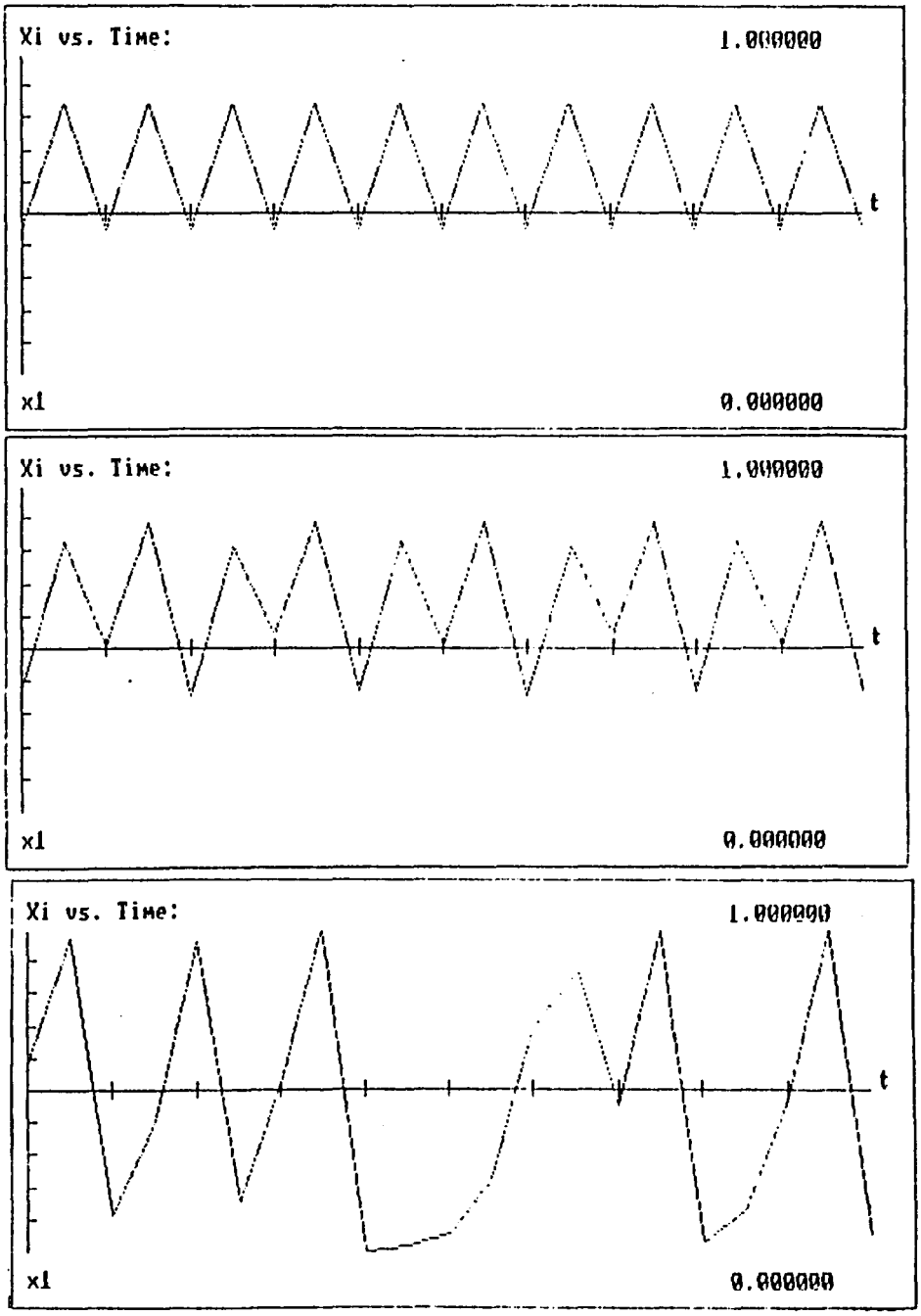

Figure 4.4: The multiple period in the logistic equation: a. period 2 for $p = 3.4$, b. period 4 for $p = 3.55$, c. nonperiodic behavior (chaos) for $p = 4.0$

iterations settle down to the alternating values of 0.45196 and 0.84215, as shown in Fig. 4.4.a. Settling to these two values is called period doubling, and 0.45196 and 0.84215 are attractors of period two. Similarly, at $p = 3.5$, there is period 4 with alternating values of 0.82694, 0.50088, 0.87500, and 0.38282, as shown in Fig. 4.4. If we increase p further, then the number of alternating values increases with period 2^n. Finally, Fig. 4.4.c shows nonalternating values at $p = 4.0$.

As mentioned in the previous paragraph, the greater the period, the faster the period doubling and the smaller the distance between neighboring points on the orbits. For example, we need a microscope to see the structure for period 2048 in the logistic maps. Higher periods have a remarkable property, which was analyzed by Mitchell Feigenbaum in the 1970s. When a period is sufficiently high, its structure is indistinguishable from the structure of the previous period. Feigenbaum found that the sequence of repeated period doubling obeys a certain law in the limit, as follows.

$$\frac{P_{d_{i+1}} - P_{d_i}}{P_{d_i} - P_{d_{i-1}}} = 0.214, \tag{4.14}$$

This number is universal as is π. Period doubling and Feigenbaum numbers appear not only on computer model simulations, but also in many kinds of natural chaos.

Concluding Remarks

So far, the mathematical concept of bifurcation theory has been reviewed. In Chapter 3, real and complex bifurcations were introduced, and in Chapter 4, Floquet theory was used to discuss periodic branch stability caused by complex bifurcation. The next two chapters apply this theory to a sample power system to explain voltage collapse and oscillatory phenomena in the framework of bifurcation theory.

CHAPTER 5. A SAMPLE THREE BUS SYSTEM

Chapters 2, 3, and 4 briefly explained the techniques necessary to study nonlinear dynamical systems in a systematic way. In this chapter, the above methods are applied to a sample electrical power system. The aim is to explain the voltage collapse process, as well as other nonlinear oscillatory phenomena a power system may undergo. To this end, the power system model (Fig. 5.1) considered by Dobson et al. [4] is employed. This model consists of a load supplied by two generators. The load is represented by an induction motor in parallel with a constant PQ load. The dynamic equations of this system consist of four state variables corresponding to the generator angle (δ), the generator angular velocity(ω), the load angle(δ_L), the load voltage magnitude (V). Load reactive power is chosen as the system parameter so that increasing Q_1 corresponds to increasing the load reactive power demand. For the detailed system equations of this model, see Appendix A.

$$\dot{\delta} = \omega \tag{5.1}$$

$$\begin{aligned} \dot{\omega} &= 16.66667\sin(\delta_L - \delta + 0.08727)V \\ &\quad - 0.16667\omega + 1.88074 \end{aligned} \tag{5.2}$$

$$\begin{aligned} \dot{\delta_L} &= 496.87181V^2 - 166.66667\cos(\delta_L - \delta \\ &\quad - 0.08727)V - 666.66667\cos(\delta_L - 0.20944)V \end{aligned}$$

$$- 93.33333V + 33.33333Q_1 + 43.33333 \tag{5.3}$$

$$\begin{aligned} \dot{V} &= -78.76384V^2 + 26.21722\cos(\delta_L - \delta \\ &\quad - 0.01241)V + 104.86887\cos(\delta_L - 0.13458)V \\ &\quad + 14.52288V - 5.22876Q_1 - 7.03268 \end{aligned} \tag{5.4}$$

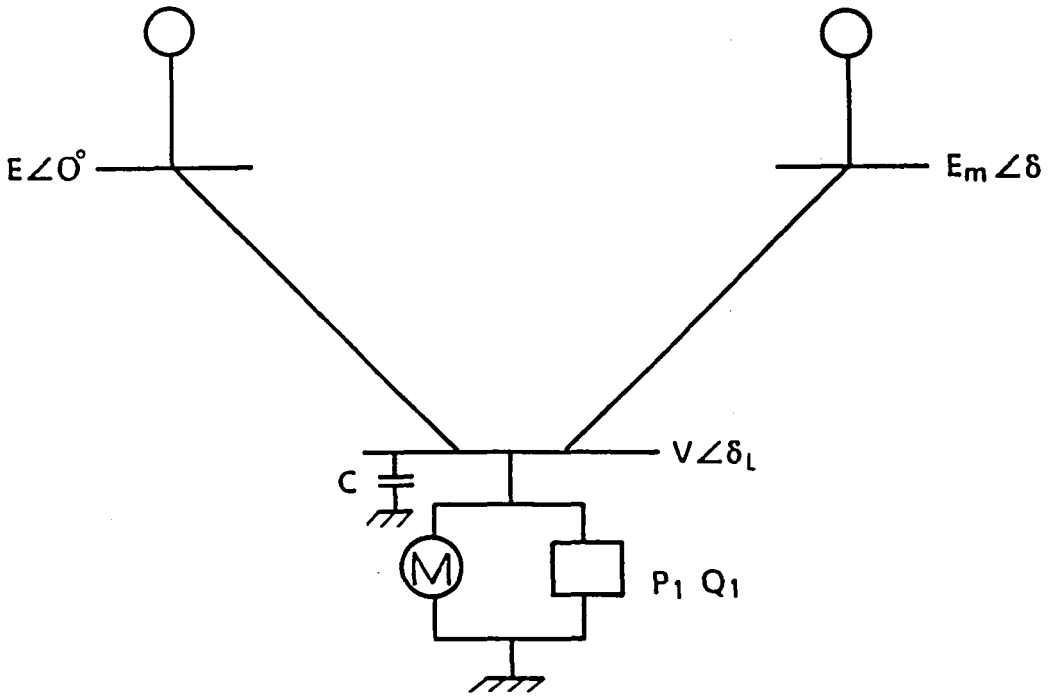

Figure 5.1: The sample power system network

The above equations can be formed as $\dot{x} = F(x,p)$, where $\dot{x}$ is the vector of four state variables, and p is the reactive power Q_1 at load bus.

In their study, Dobson et al. [4] determined only the voltage collapse phenomenon in the sample power system model and missed other nonlinear phenomena. This chapter analyze the nonlinear oscillatory phenomena not reported in their work.

Computing Stationary Branch

Suppose the power system described by Eqs. 5.1, 5.2, 5.3, and 5.4 is operating at the stable equilibrium point $x_s(Q_1)$, where Q_1 is the reactive power demand at the load bus. Now, assume that Q_1 is slowly increased while other parameters remain fixed. In such an instance, equilibrium point $x_s(Q_1)$ will vary as Q_1 is increased. At each parameter step, the system eigenvalues are calculated in the anticipation of identifying critical points at which the real part of certain eigenvalues become zero. As mentioned in Chapter 3, the critical point corresponding to Hopf bifurcation has a complex conjugate pair with zero real part. On the other hand, the critical point representing real bifurcation has a zero real eigenvalue.

Obtaining the stationary branch is straightforward as long as the steady-state equilibrium point is at a distance from real bifurcation. The algebraic system determining the equilibrium point, however, will be ill-conditioned when it approaches real bifurcation. In fact, this critical point is often defined as the point at which the Jacobian of the Newton-Raphson method becomes singular. To avoid this singularity, the continuation method is applied. Thus, the resulting continuation algorithm avoids becoming ill-conditioned and instead approximates the critical point.

The software package *AUTO* [16] provides the continuation algorithm, and also

Table 5.1: State Variable Values At The Critical Points

δ	ω	δ_L	V	Q_1	
0.31009	0.0	0.12005	1.09991	10.94606	S_1
0.34348	0.0	0.13620	0.94252	11.40678	S_2
0.34755	0.0	0.13799	0.92501	11.41146	S_3

automatically calculates eigenvalues at each parameter step. The numerical results shown in the preceding section were calculated by this package.

Detecting the Critical Points

In the course of computing a stationary branch, three critical points are detected, as shown in Table 5.1. Figure 5.2 shows the stationary branch and the three critical points–S_1, S_2, and S_3–at which the system changes its stability. The critical points correspond to an operating point at which certain eigenvalues of the system cross the imaginary axis. In Fig. 5.2, the solid line represents the stable state, and the dotted line the unstable stationary trajectory.

Table 5.2 shows the variations of system eigenvalues when the parameter Q_1 is varied. The real part of complex conjugate eigenvalues becomes positive through S_1 and then negative again through S_2. After a short stable region, one real eigenvalue becomes positive at S_3. There are no point attractors in the interval between S_1 and S_2. At two critical points–S_1 and S_2–a pair of complex conjugate eigenvalues cross the imaginary axis, as shown in Fig. 5.3. At the last critical point, S_3, also called the fold bifurcation point or the turning point, one real eigenvalue becomes zero.

In this chapter, the critical points S_1 and S_2 are studied in detail. At these

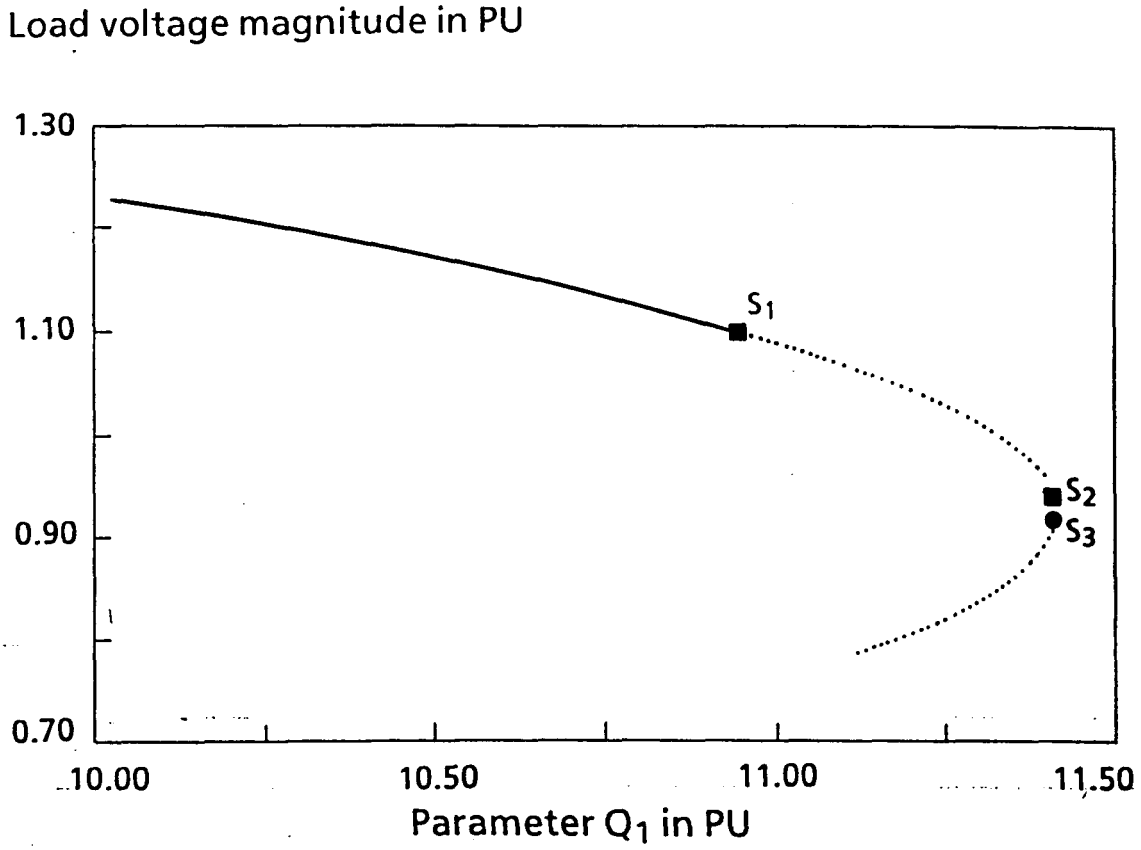

Figure 5.2: A QV curve in a sample power system

Table 5.2: The movement of eigenvalues

$Real_1$	$ComplexConjugate$	$Real_2$	
-0.13459E+03	-0.10548E-01±j 0.38004E+01	-0.16889E+02	
-0.13154E+03	-0.54156E-02±j 0.37742E+01	-0.16133E+02	
-0.13019E+03	-0.29641E-02±j 0.37622E+01	-0.15788E+02	
-0.12927E+03	-0.12323E-02±j 0.37539E+01	-0.15550E+02	
-0.12863E+03	-0.15137E-05±j 0.37481E+01	-0.15384E+02	S_1
-0.12673E+03	0.38559E-02 ±j 0.37302E+01	-0.14879E+02	
-0.12375E+03	0.10479E-01 ±j 0.37008E+01	-0.14061E+02	
-0.12002E+03	0.19873E-01 ±j 0.36611E+01	-0.12993E+02	
-0.11774E+03	0.26326E-01 ±j 0.36348E+01	-0.12312E+02	
-0.11533E+03	0.33828E-01 ±j 0.36049E+01	-0.11567E+02	
-0.11275E+03	0.42683E-01 ±j 0.35699E+01	-0.10741E+02	
-0.10996E+03	0.53296E-01 ±j 0.35273E+01	-0.98087E+01	
-0.10687E+03	0.66155E-01 ±j 0.34726E+01	-0.87300E+01	
-0.10336E+03	0.81411E-01 ±j 0.33958E+01	-0.74326E+01	
-0.99158E+02	0.95124E-01 ±j 0.32687E+01	-0.57587E+01	
-0.95188E+02	0.78427E-01 ±j 0.30807E+01	-0.39933E+01	
-0.93613E+02	0.43327E-01 ±j 0.29742E+01	-0.31992E+01	
-0.92606E+02	-0.36278E-03 ±j 0.28937E+01	-0.26368E+01	S_2
-0.90789E+02	-0.16853E+00 ±j 0.27402E+01	-0.14191E+01	
-0.89119E+02	-0.45468E+00 ±j 0.27318E+01	-0.73737E-02	S_3
-0.87257E+02	-0.64046E+00 ±j 0.29305E+01	0.13355E+01	
-0.85549E+02	-0.67057E+00 ±j 0.30956E+01	0.23204E+01	
-0.84035E+02	-0.65205E+00 ±j 0.32010E+01	0.31324E+01	
-0.82697E+02	-0.62111E+00 ±j 0.32672E+01	0.38445E+01	

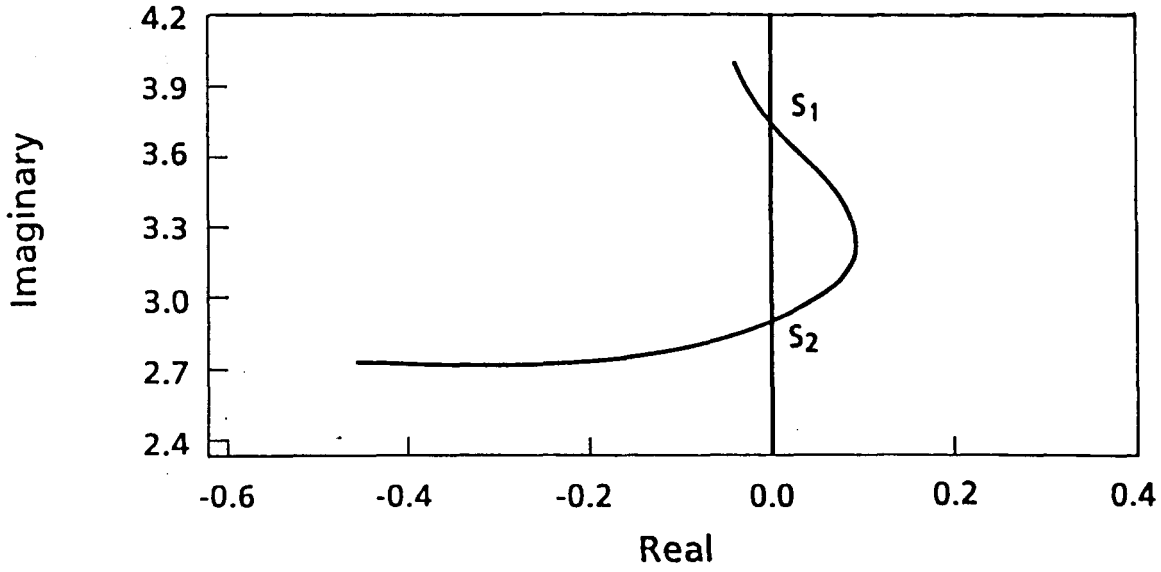

Figure 5.3: The movement of the complex conjugate eigenvalue

points, the possibility of oscillatory or of other nonlinearly dynamic behavior is investigated by applying the Hopf and Floquet theories. System behavior near S_3 may be associated with voltage collapse and will be discussed in the next chapter.

Checking for Hopf Bifurcation Conditions

In the previous section, we detected the points S_1 and S_2, at which the real parts of complex conjugate eigenvalues become zero. The eigenvalues at the first two critical points–S_1 and S_2–are {0.0000 ± j3.7481, -128.6327, -15.3845} and {0.0000 ± j2.8937, -92.6059, -2.6365}, respectively. The complex conjugate pair of eigenvalues correspond to generator angle and to generator–angular velocity, respectively.

The existence of Hopf bifurcation is verified by satisfying the conditions men-

tioned in Chapter 3. The stability of Hopf bifurcation is verified by calculating the value β_2, which is calculated by the package *BIFOR2* [12].

$$At S_1,\ \beta_2 = 0.0904025 \quad (subcritical),$$

and

$$At S_2,\ \beta_2 = -252.2531 \quad (supercritical).$$

The periodic branch emanating from S_1 is locally unstable because it is subcritical, whereas the periodic branch emanating from S_2 is locally stable because it is supercritical.

This condition is local in terms of fixing the parameter at the Hopf bifurcation point. Further increases of the parameter move the system state along the periodic orbit emanating from the Hopf bifurcation. The next section explains system behavior along this trajectory.

Tracing the Periodic Branch

As mentioned in Chapter 4, Floquet multipliers calculated from the monodromy matrix provide useful information for analyzing the stability of the periodic orbit. Table 5.3 shows the movement of Floquet multipliers along the branch of periodic orbit in between S_1 and S_2. $FL_i, (i = 1, \cdots, 4)$ and *NUMBER*, respectively, represent four Floquet multipliers and the number of Floquet multipliers inside the unit circle. The same *AUTO* package used here to trace periodic orbits generates the Floquet multipliers automatically at each parameter step. Figs. 5.4 and 5.5 show the branching diagram of parameter space, which includes periodic orbits. These figures depict the branch of stationary solutions including the unstable part and the point at

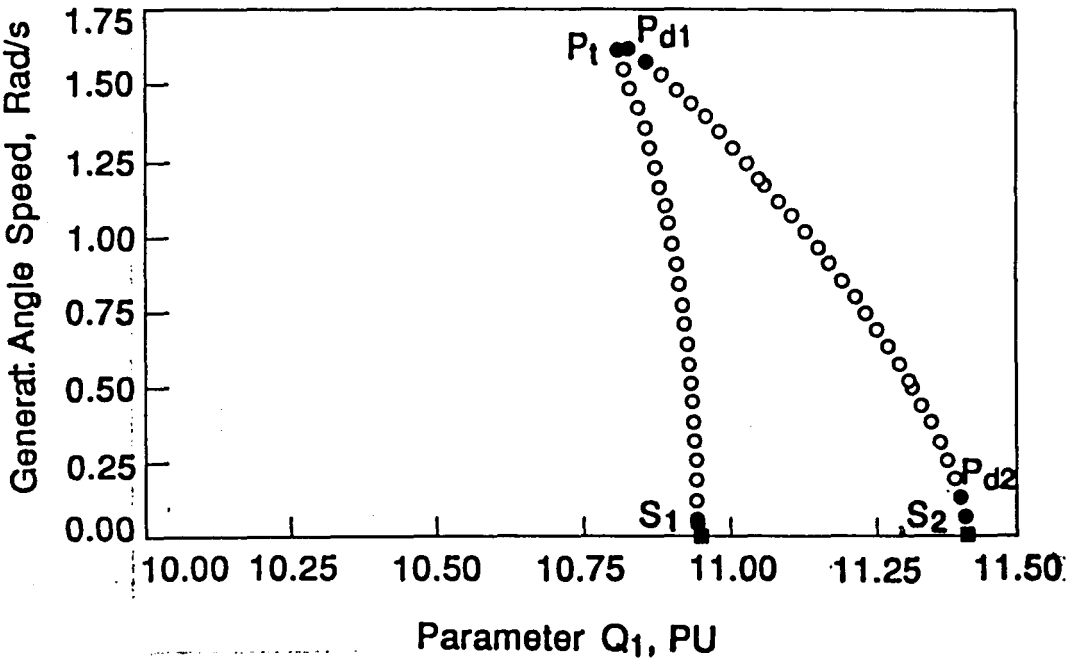

Figure 5.4: The branching diagram of ω-Q_1

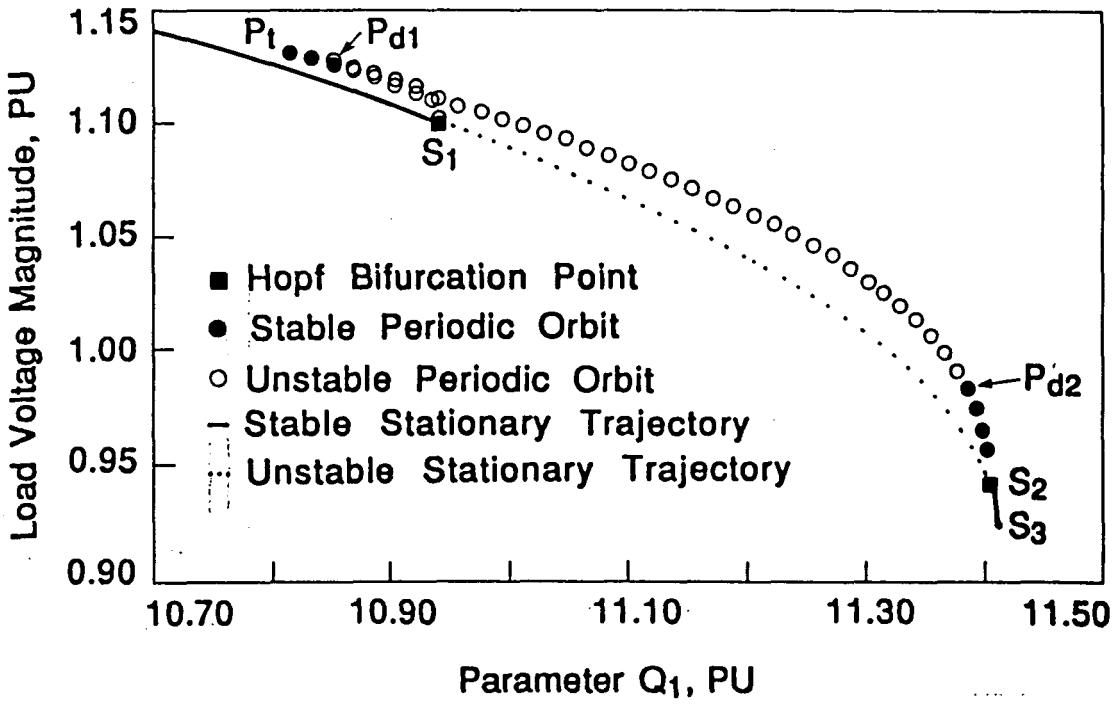

Figure 5.5: The branching diagram of V-Q_1

Table 5.3: The movement of floquet multipliers

FL_1	FL_2	FL_3	FL_4	NUMBER	B.Pt.
1.00	1.01	0.00	0.00	3	
1.00	1.06	0.00	0.00	3	
1.00	0.93	0.00	0.00	4	P_t
1.00	0.60	0.00	0.00	4	
1.00	-0.43	0.00	0.00	4	
1.00	-0.93	0.00	0.00	4	
1.00	-1.50	0.00	0.00	3	P_{d1}
1.00	-10.59	0.00	0.00	3	
1.00	-30.87	0.00	0.00	3	
1.00	-1.01	0.00	0.00	3	
1.00	-0.50	0.00	0.00	4	P_{d2}
1.00	0.35	0.00	0.00	4	
1.00	0.97	0.00	0.00	4	

which the two Hopf bifurcation points are connected by a branch of periodic orbits. The stable–steady state solution becomes unstable for the value $Q_1 = 10.94606$, and a periodic limit cycle emanates from Hopf bifurcation point S_1. At this point, the periodic solution has a frequency of $f_1 = 0.596527$ and a period of $T_1 = 1.67637$, which is associated with the imaginary part of complex conjugate eigenvalues obtained from the system equations. The periodic branch S_1 to P_t emanating from S_1 is unstable because it is subcritical and because one of the multipliers lies outside the unit circle. As can be seen from the same diagram (Figs. 5.4 and 5.5), at point P_t, the multiplier lying outside the unit circle enters the unit circle from the positive side of the real axis, and the unstable periodic orbit turns to the right and gains stability. With further increases of Q_1, however, one of the multipliers crosses the unit circle at -1 for the value of $Q_1 = 10.8716$ and this periodic orbit bifurcates to a new periodic orbit with period two. The multiplier enters the unit circle again

from the negative side of the real axis for the value of $Q_1 = 11.38847$, which is the period–doubling bifurcation point P_{d_2}. When the multiplier passes through the second period–doubling bifurcation point P_{d_2}, again the periodic orbit gains stability in the supercritical region between P_{d_2} and S_2. Finally, system oscillation vanishes at S_2 ($Q_1 = 11.40678, f_2 = 1.060985$), and the system state approaches the critical point S_3.

The stability and the type of periodic bifurcation solution, as mentioned above can be explained in terms of the movement of Floquet multipliers. Each predicted behavior in this section will be verified through time simulation.

Bistable Region

As shown in Figs. 5.4 and 5.5, at the interval $10.84041 < Q_1 < 10.88559$, there exist two stable attractors: one is the steady state, and the other a stable limit cycle. The simultaneous existence of two stable attractors raises quite interesting questions including that of as which attractor dominates system behavior.

This question can be answered by considering points A, B, and C in Fig. 5.6. These points correspond to the value $Q_1 = 10.85$, where $10.84061 < Q_1 < 10.88559$. The point labeled A corresponds to a stable fixed point; B, to an unstable limit cycle; and C, to a stable limit cycle. For the value Q_1, the system has a stable equilibrium point surrounded in the phase plane by an unstable limit cycle, which is in turn surrounded by a stable limit cycle, with the unstable limit cycle acting as the separatrix between the basin of attraction of the equilibrium point and that of the stable limit cycle. Thus, the perturbed system lying inside the unstable limit cycle will tend towards the fixed point, whereas the perturbed system lying outside

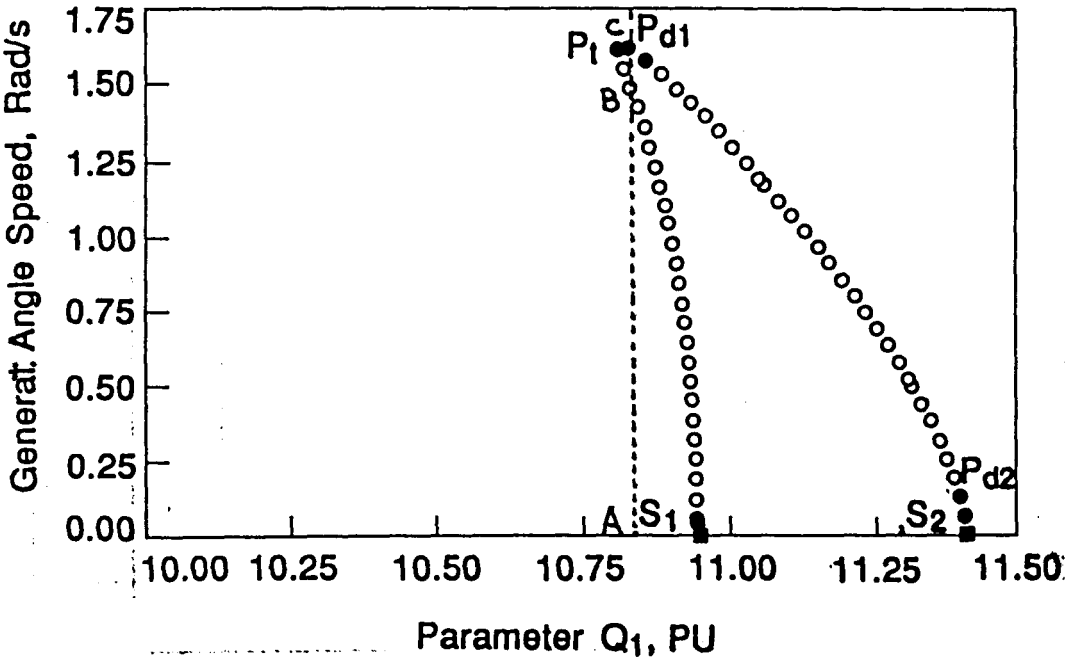

Figure 5.6: The bistable branch in the bifurcation diagram

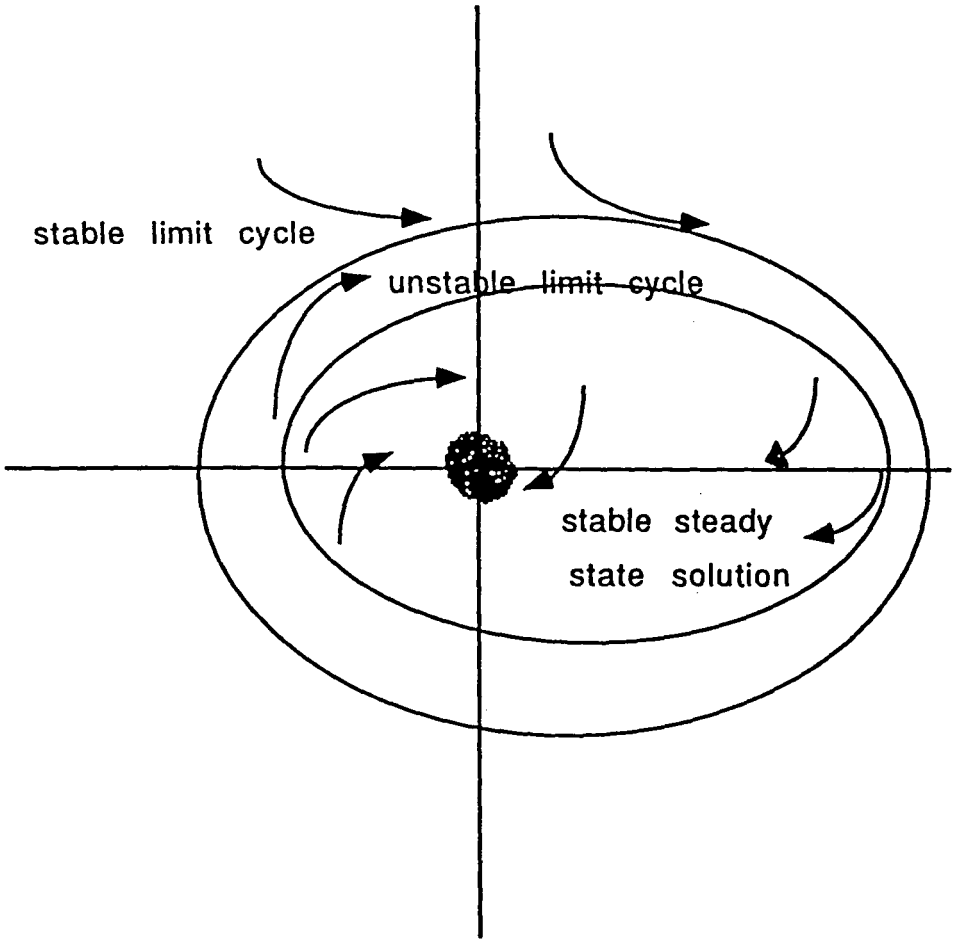

Figure 5.7: Two attractors and an unstable limit cycle

this region will tend towards the stable limit cycle. This bistability is illustrated in Fig. 5.7, which shows a ω–δ plot of the phase plane for $Q_1 = 10.85$.

A Series of Period–doubling Bifurcations

The sample time simulation of such predicted behavior with respect to growing oscillation near S_1, period two oscillation at P_{d_2}, and period one oscillation between P_{d_2} and S_2 is shown in Figs. 5.8 through 5.12. Figure 5.8 shows a growing oscillation for $Q_1 = 11.0245$ near S_1. Figures 5.9 and 5.10 show the single period oscillation for $Q_1 = 11.389$ on the S_2 to P_{d_2} branch. Figures 5.11 and 5.12 show the period two oscillation for $Q_1 = 11.383$ near P_{d_2}, with two different maximum amplitudes.

As mentioned in Chapter 2, according to the bifurcation theory, one way to chaotic motion is through a sequence of period–doubling bifurcations. Figures 5.13 and 5.14 show period four oscillation for $Q_1 = 11.380$. The chaotic motion captured at $Q_1 = 11.379$ is shown in Figs. 5.15 and 5.16. Near the period–doubling bifurcation point P_{d_2}, because of the stiffness of the generator angle and the generator angular velocity with respect to parameter Q_1, the oscillation is very sensitive to the parameter value, as can be seen in Figs. 5.11 through 5.16.

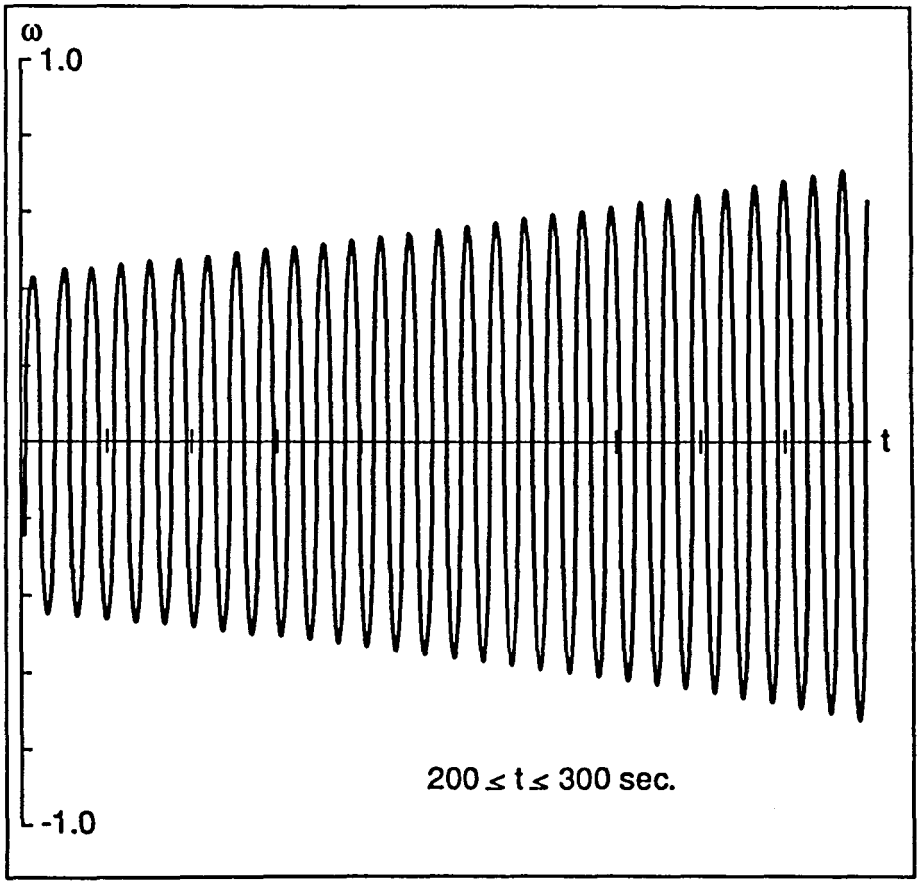

Figure 5.8: Growing oscillation for $Q_1 = 11.0245$

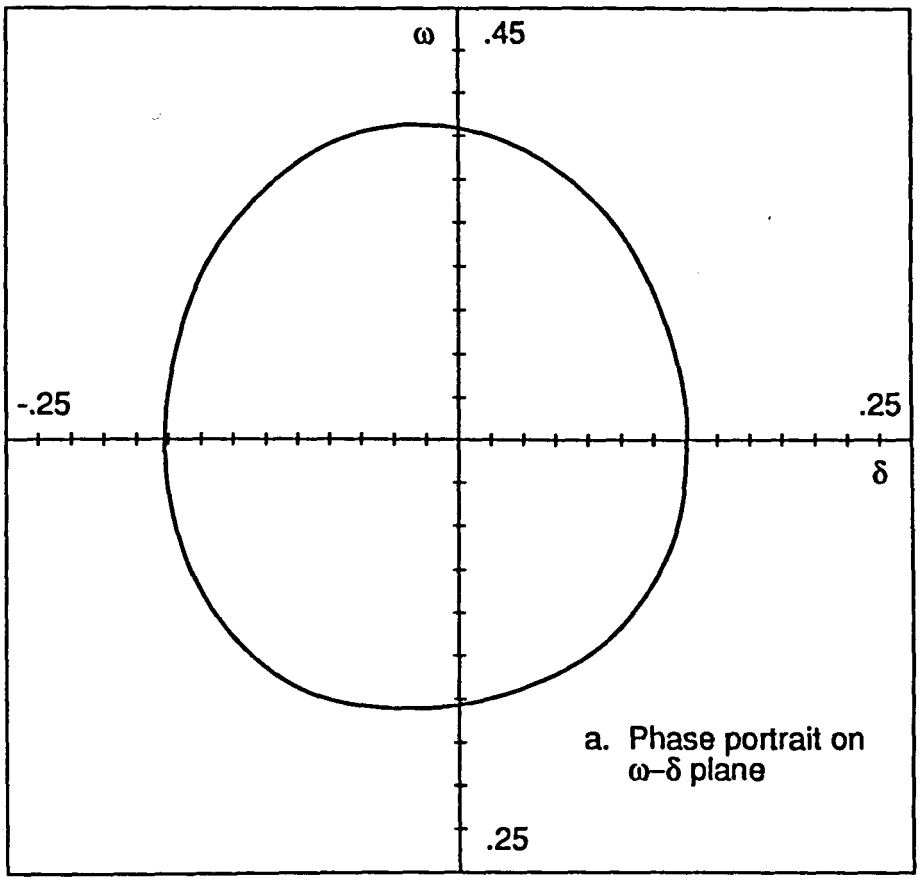

Figure 5.9: ω–δ phase plane trajectory: Period one oscillation for $Q_1 = 11.389$

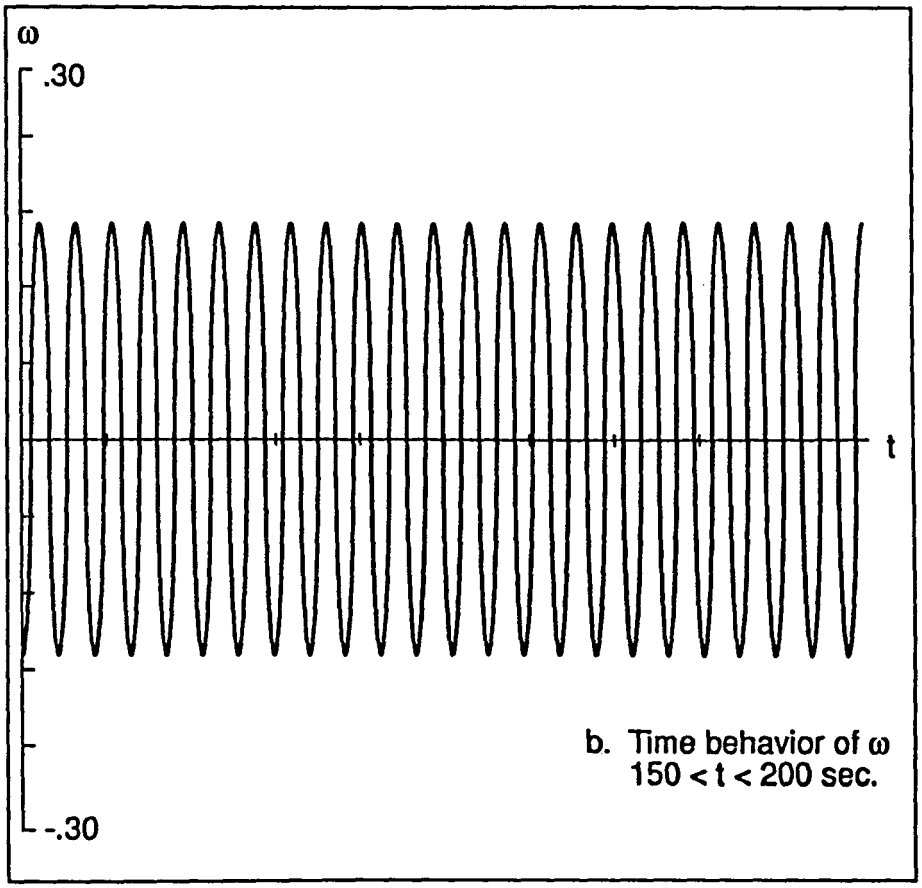

Figure 5.10: ω in time axis: Period one oscillation for $Q_1 = 11.389$

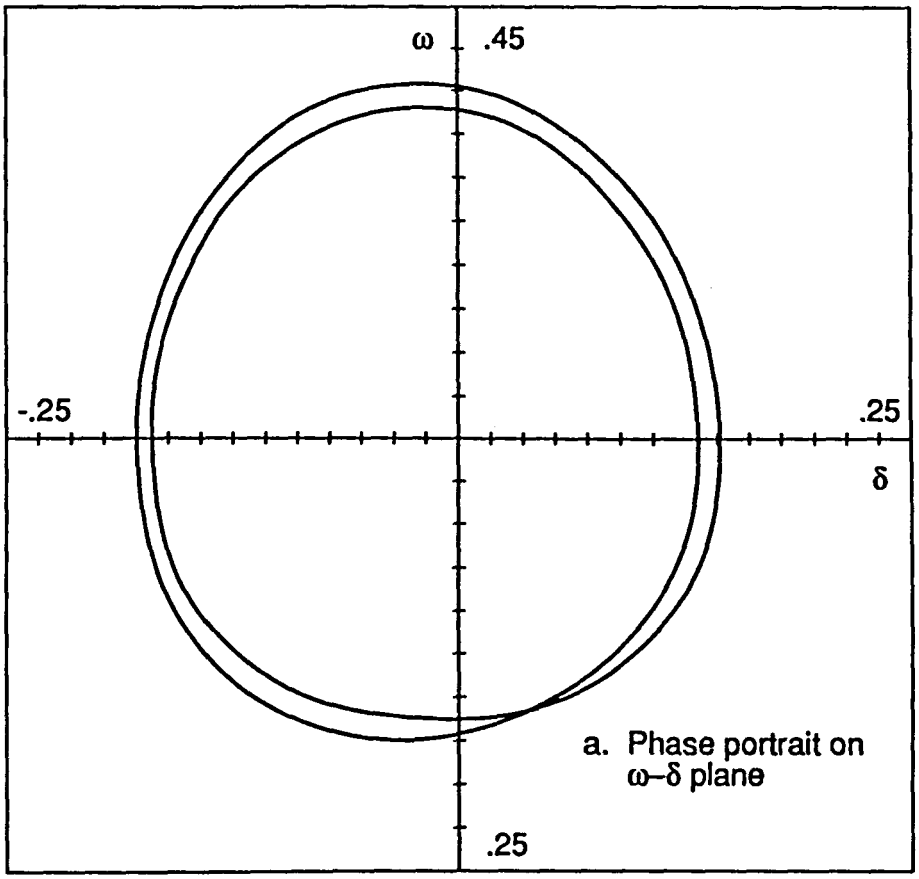

Figure 5.11: ω–δ phase plane trajectory: Period two oscillation for $Q_1 = 11.383$

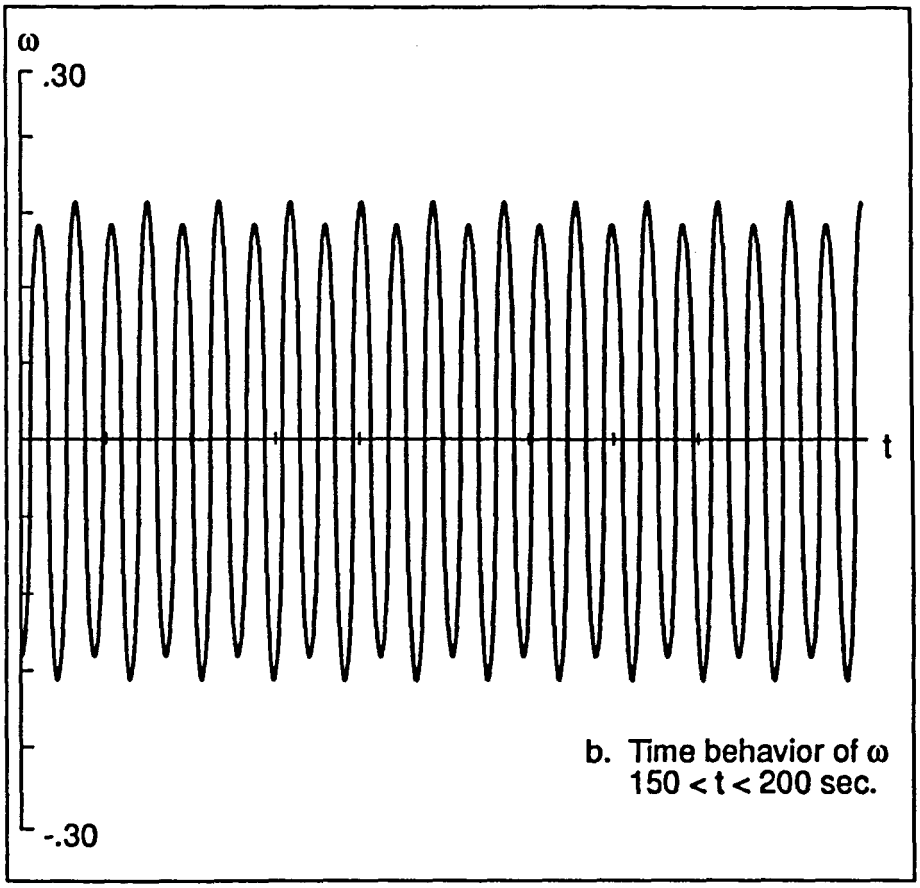

Figure 5.12: ω in time axis: Period two oscillation for $Q_1 = 11.383$

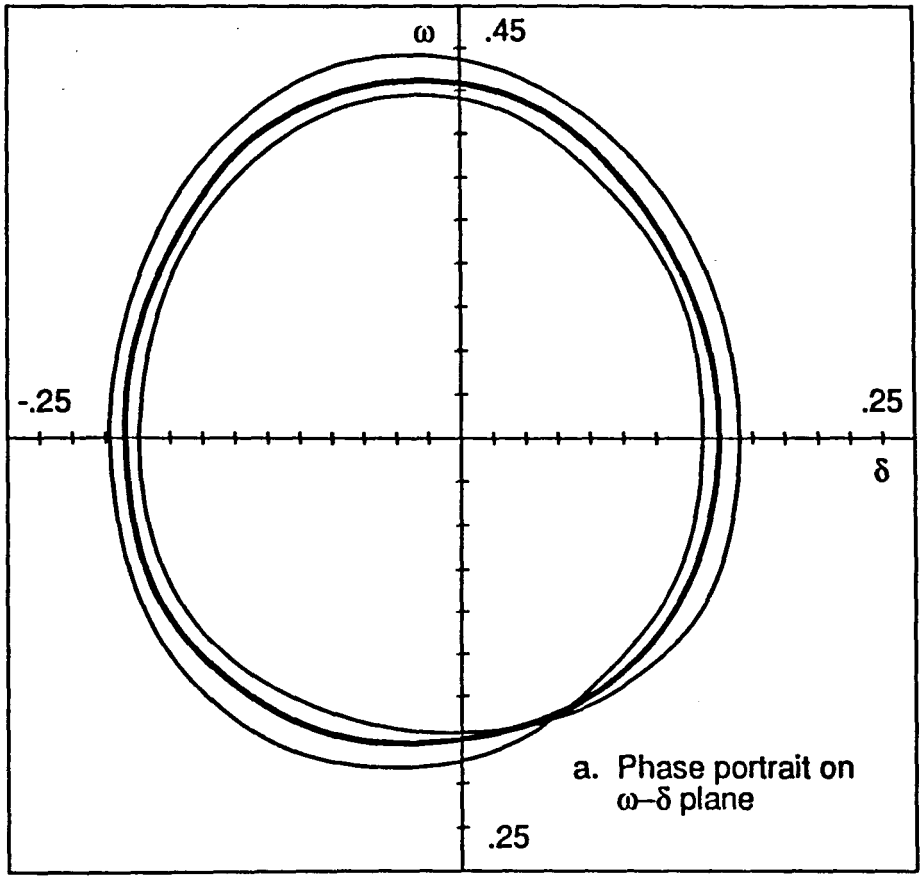

Figure 5.13: ω–δ phase plane trajectory: Period four oscillation for $Q_1 = 11.380$

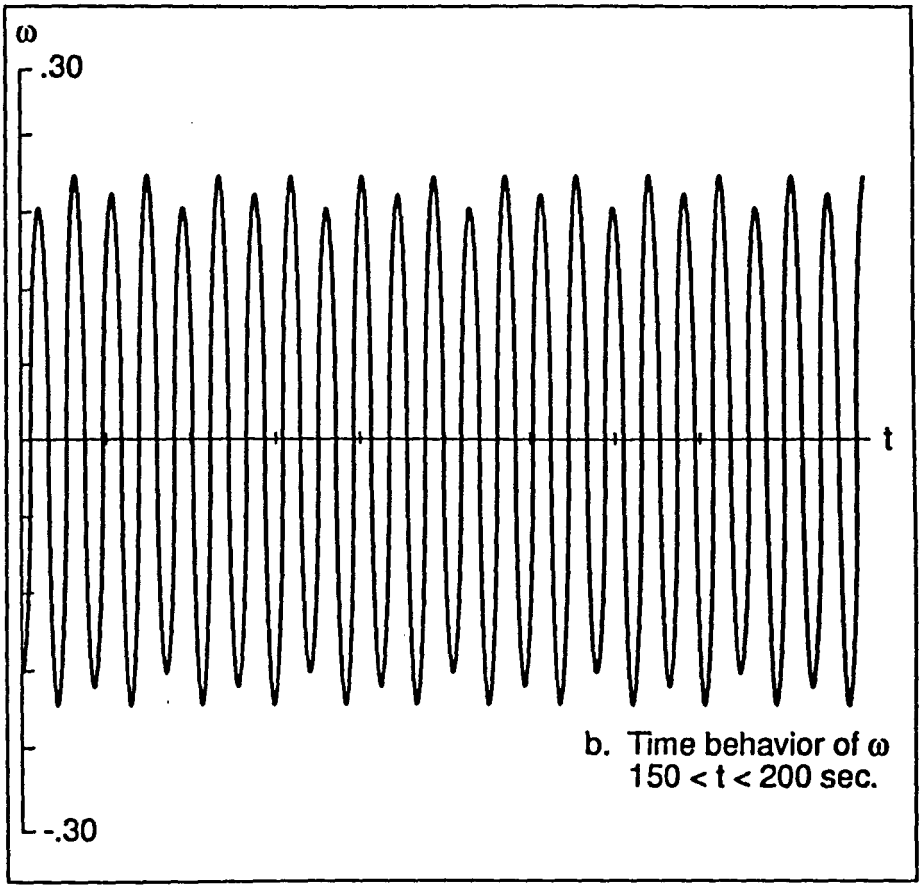

Figure 5.14: ω in time axis: Period four oscillation for $Q_1 = 11.380$

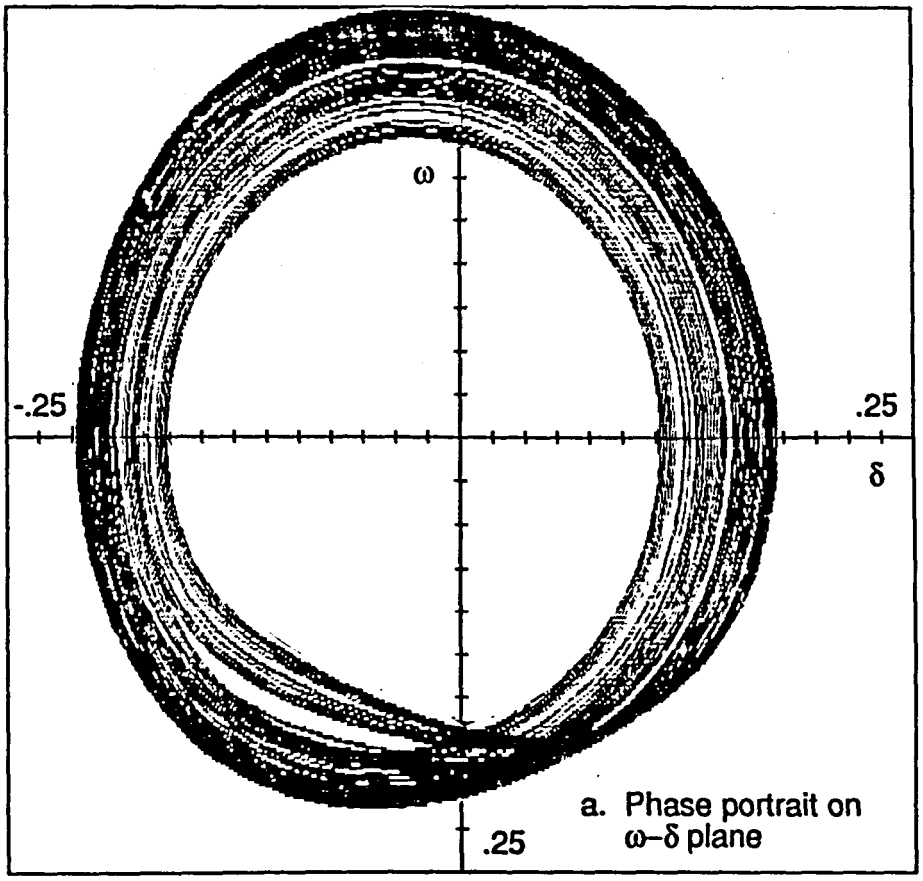

Figure 5.15: ω–δ phase plane trajectory: Chaotic behavior for $Q_1 = 11.379$

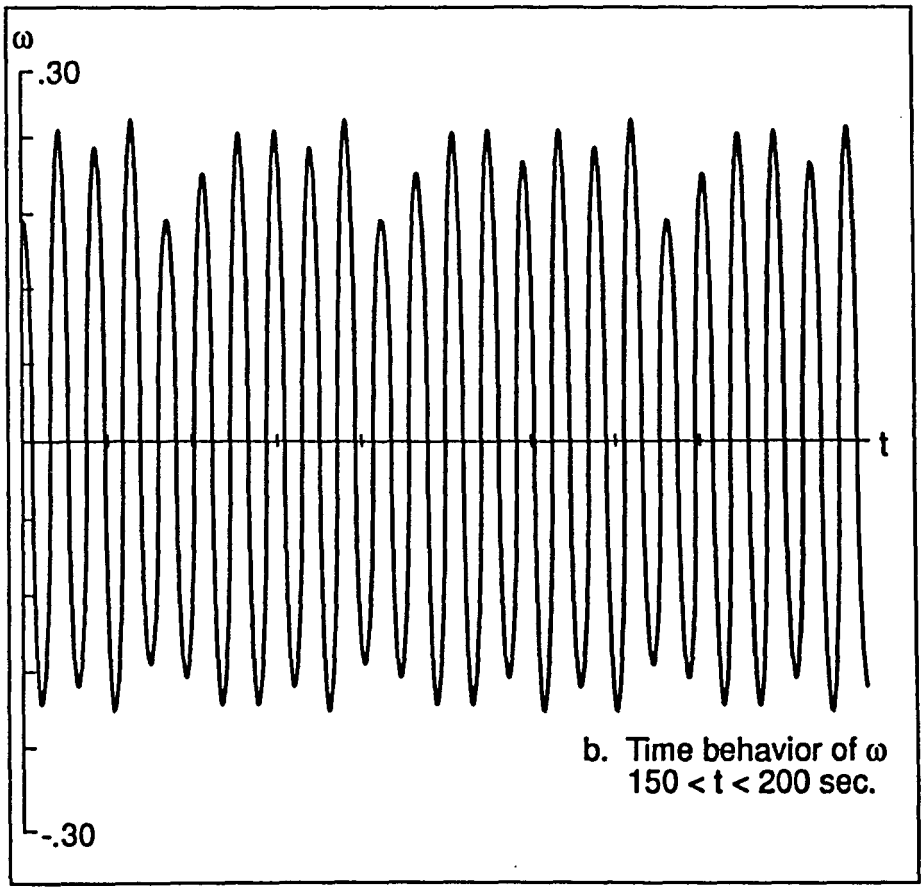

Figure 5.16: ω in time axis: Chaotic behavior for $Q_1 = 11.379$

Additional Remarks

In this chapter, we verified oscillatory phenomena through time simulations with *PHASER*, a simulator devised for dynamical systems [13]. To analyze chaotic oscillation theoretically, however, pertinent methods are required. Types of analyses still needed in the study of chaos will be mentioned at the conclusion of this thesis.

CHAPTER 6. VOLTAGE COLLAPSE AND CENTER MANIFOLD REDUCTION

In the previous chapter, we discussed system behavior in the region before critical point S_3. The oscillation phenomenon vanishes when load reactive power Q_1 is further increased through the second Hopf bifurcation point S_2. Additional increases in Q_1 are possible only up to S_3, beyond which the voltage may collapse.

Dobson et al. [4] investigated system dynamics near the point S_3 and suggested a voltage collapse model based on center manifold. The results of their study and of ours are briefly summarized and compared in the next section. They considered the complete system model, whereas our study concentrates on a reduced model obtained through the center manifold reduction technique.

Review of the Previous Work

Dobson et al. [4] suggested that voltage collapse can be identified in system dynamics at a saddle–node bifurcation (fold bifurcation) of a stable equilibrium point. They developed the model of generator and load dynamics described in the Appendix A.

At point S_3, the Jacobian matrix evaluated has one zero real eigenvalue, and the real parts of the remaining ones are negative. The eigenvector corresponding to

the zero real eigenvalue points in the direction of system trajectories. A curve is made up of the system trajectories, which are tangential to the eigenvector at S_3 and which are the union of a system trajectory converging to S_3 (W^c_-), the equilibrium point S_3, and a system trajectory diverging from S_3 (W^c_+). Thus S_3 is stable for the initial conditions on W^c_- and unstable for the initial conditions on W^c_+. The sign of the eigenvector is chosen so that it points along the system trajectory diverging from S_3. Because the nonzero eigenvalues of the Jacobian at S_3 have negative real parts, the eigenvector points along the only unstable direction. Because S_3 is unstable, a small perturbation of the state from S_3 may cause the state to move away from S_3 in the approximate direction of the eigenvector.

The values of state variables at S_3 are $(\delta^*, \omega^*, \delta^*_L, V^*)$ = (0.34755, 0.0, 0.13799, 0.92501), and Q_1 = 11.41146. The eigenvector associated with the zero eigenvalue at S_3 is $(0.235, 0.0, 0.102, -1.000)$. The relatively large negative component of the eigenvector associated with voltage indicates that, at S_3, the initial movement of system dynamics will be in such a direction that voltage magnitude decreases while other state variables remain nearly constant.

Numerically, system dynamics at S_3 are identified by numerical integration methods designed for stiff systems, because the Jacobian of the system is quite ill-conditioned around S_3. Figure 6.1 shows the behavior of voltage magnitudes at the critical point, with respect to time. It starts with a slow variation and at some instance drops abruptly.

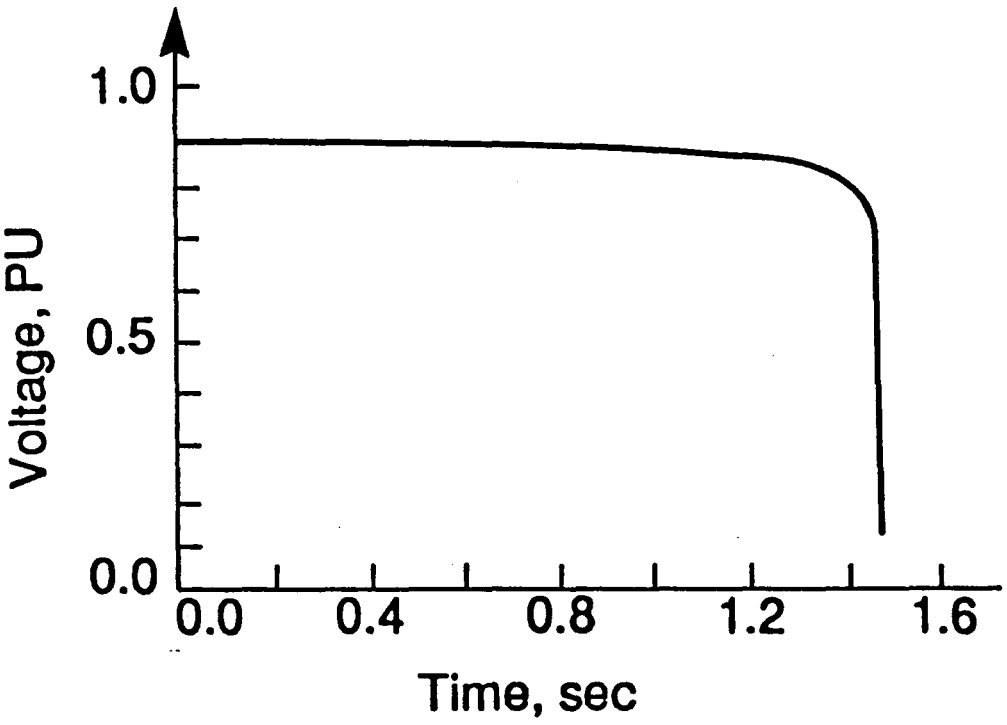

Figure 6.1: The behavior of voltage at S_3: The magnitude of voltage at the critical point of the complete system

Center Manifold Reduction

In the previous section, system dynamics involved in the voltage collapse process were demonstrated. As discussed in Chapter 3, the same dynamical behavior can be observed qualitatively with a reduced number of system equations. In this section, the original dynamic equations with four state variables are reduced to a form with

only one critical variable.

As mentioned earlier, the dynamical system model has four state variables– $\delta, \omega, \delta_L, V$–and a single parameter corresponding to load reactive power Q_1. At S_3, the system becomes critical with the value

$$x_C = \begin{pmatrix} 0.34755 & 0.0 & 0.13799 & 0.92501 \end{pmatrix}$$

$$p_C = \begin{pmatrix} 11.41146 \end{pmatrix}.$$

Eigenvalues corresponding to the critical state are $(0.0000, -89.1100, -0.4562 \pm j2.7325)$, at which the real eigenvalue becomes zero although the other eigenvalues have negative real parts.

When new variables are introduced, all critical values of state variables and value of a parameter are shifted to the origin

$$\dot{z} = F_1(z, u), \tag{6.1}$$

where

$$z = x - x_C \tag{6.2}$$

$$u = p - p_C. \tag{6.3}$$

Now, the transformation

$$Y = T^{-1} z \tag{6.4}$$

gives Eq. 6.1 the new coordinates

$$\dot{y} = F_2(y, u), \tag{6.5}$$

where T is a nonsingular transformation matrix containing eigenvectors of function F at the critical point, as follows:

$$T = \begin{pmatrix} 0.2349 & -0.0019 & 0.0594 & 0.3560 \\ 0.0001 & 0.1730 & -1.0000 & 0.0000 \\ 0.1020 & -1.0000 & 0.0300 & 0.1806 \\ -1.0000 & 0.0566 & -0.3672 & 0.0234 \end{pmatrix}.$$

An NAG subroutine F02AGF on the VAX/VMS 11/780 system was used to calculate eigenvalues of function F at S_3. Now the Jacobian of function F_2 will be in the Jordan Canonical form

$$\begin{pmatrix} \dot{Y}_c \\ \dot{Y}_s \end{pmatrix} = \begin{pmatrix} B & 0 \\ 0 & C \end{pmatrix} \begin{pmatrix} Y_c \\ Y_s \end{pmatrix} + \begin{pmatrix} G_1(Y_c, Y_s, u) \\ G_2(Y_c, Y_s, u) \end{pmatrix},$$

where

$$B = (0.0000),$$

$$C = \begin{pmatrix} -89.1100 & 0.0000 & 0.0000 \\ 0.0000 & -0.4562 & 2.7325 \\ 0.0000 & -2.7325 & -0.4562 \end{pmatrix}.$$

All algebraic manipulation is performed with the symbolic calculation software-package MACSYMA. As explained previously, y_C can be incorporated into y_S, as shown in Eq. 3.9. If we take the second-order approximation of Eq. 3.9, then it can be directly obtained from Eq. 3.10 without solving the nonlinear Eq. 3.11 which consists of coefficients of Eq. 3.9. In as much as the equations involve trigonometric functions, they create multitude of extra terms in the process of algebraic manipulation. Finally, the four-dimensional system is reduced into a form having only one

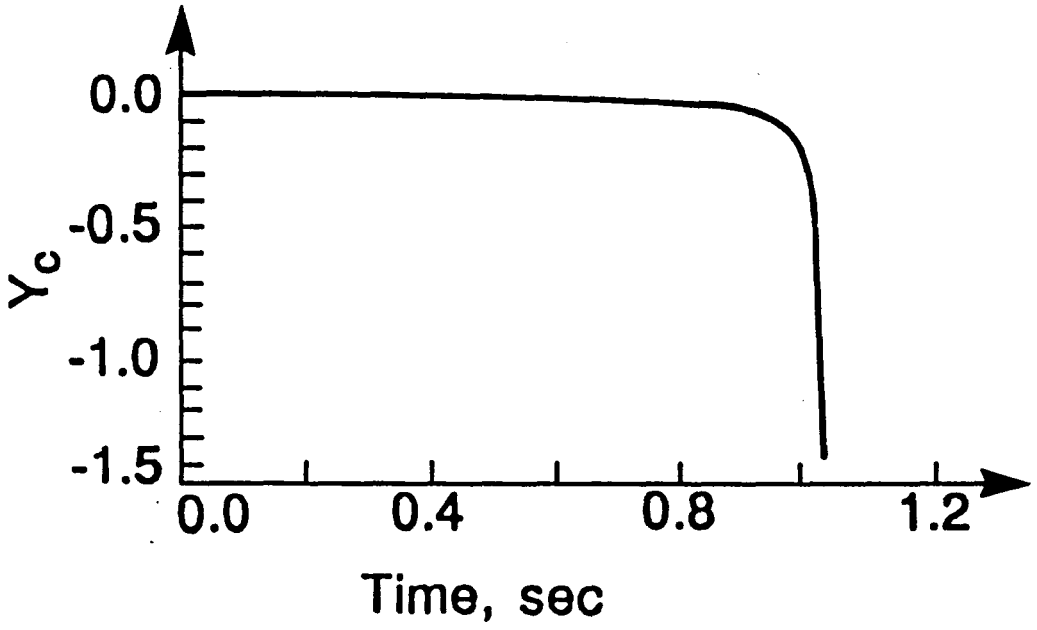

Figure 6.2: The behavior of voltage at S_3: The variation of the center manifold variable

critical variable:

$$\dot{y}_C = -81.819890 y_C^2, \tag{6.6}$$

where y_C is a combination of four state variables. The results of the time simulation in Fig. 6.2 approximate well the time simulation curve for the complete system.

CHAPTER 7. SUGGESTIONS FOR FUTURE WORK AND CONCLUSIONS

Suggestions for Future Work

In this thesis, the nonlinear power system dynamical model is studied in the framework of bifurcation theory. The motivation for this study was recent advances in both nonlinear dynamics and chaos theory. The important outcome of chaos theory is that even a simple deterministic model is capable of extremely complicated behavior. Preliminary study of a sample power system dynamic model indeed confirmed this possibility. To be realistic, however, the theory must be extended to large, practical power system networks with detailed network models. To this end, a robust continuation methodology tracking steady-state solution trajectory must first be developed. This methodology has already been developed in the form of a continuation power flow package [17] based on Rheinboldt and Burkardt's study [18] and is capable of handling large systems. Similarly, a methodology tracking periodic solution and their stability can be developed based on Floquet theory.

Conclusions

In general, solving or analyzing nonlinear dynamical equations is quite difficult and requires special techniques. To overcome such difficulties, systems are gener-

ally linearized in an attempt to predict their behavior. The study described in this thesis stressed the importance of nonlinearity in power system dynamics, especially in highly stressed systems. Recent advances in bifurcation and nonlinear dynamical system theories have made it possible to analyze dynamical systems systematically. The examples included in this work have shown the importance of bifurcation theory in the analysis of nonlinear dynamical equations. In the early stage of our research, we in fact applied this theory to the power system example to analyze the dynamic aspects involved in the voltage collapse process. During theory testing, it was discovered that other types of bifurcations were possible. For example, the study revealed the existence of both stable and unstable periodic orbits for certain values of the parameter under consideration. Periodic orbits and their stability were therefore studied in the framework of Hopf bifurcation and Floquet theory. The predicted behavior was verified by softwares such as *AUTO, BFIRO2, MACSYMA*, and *PHASER.* It was concluded that the voltage collapse phenomenon is a subset of overall bifurcation phenomena.

Certain aspects of the work reported in this thesis, chaos, for example, have not yet been observed in a significant way in practical power system networks. Erratic nonlinear oscillation attributed to noise in the system, however, has been observed. The analysis developed in this study may lead to an explanation of noise from chaos.

Nonlinear dynamics theory is not yet complete, and much research is being done in the United States and abroad. This thoery can do much to improve the ability of power system engineers to tackle the problems of voltage collapse and of nonlinear oscillations.

BIBLIOGRAPHY

[1] Vittal, V., N. Bhatia, and A. A. Fouad. "Analysis of The Inter–Area Mode Phenomenon in Power Systems Following Large Disturbance." *Paper no. 91WM228-7PWRS.* IEEE Winter Power Meeting, New York, Feb., 1991.

[2] Tamura, Y., N. Yorino, and S. Iwamoto. "On the Possibility of Parametric Resonance in Power Systems." *A New Concept of Power System Stability*, Proc. PSCC 8 (1984): 939.

Frequency

[3] Thomas, R. J. and A. Tiranuchit. "Dynamic Voltage Instability." *IEEE Proceedings of 26th Conference on Control and Decision.* Los Angeles, CA., Dec. 1987.

[4] Dobson, Ian, Hsia-Dong Chiang, James S. Thorp, and Lazhar Fekih-Ahmed. "A Model of Voltage Collapse in Electric Power Systems." *IEEE Proceedings of 27th Conference on Control and Decision,* Austin, TX., Dec. 1988.

[5] Abed, E. H. and P. P. Varaiya. "Nonlinear Oscillations in Power Systems." *Int. J. Electr. Power and Energy System*, 6 (1984): 37–43.

[6] Alexander J. C. "Oscillatory Solution of a Model System of Nonlinear Swing Equation." *Int. J. Electr. Power and Energy System* , 8 (1986): 130–136.

[7] Rajagopalan, C., P. W. Sauer, and M. A. Pai. "Analysis of Voltage Control System Exhibiting Hopf Bifurcation." *IEEE Proceedings of 28th Conference on Decision and Control,* Tampa, Florida, Dec. 1989.

[8] Ajjarapu, V. and B. Lee. "Nonlinear Oscillations and Voltage Collapse Phenomena in an Electrical Power System." Proceedings of the 22nd North America Power Symposium, Auburn, Alabama, Oct. 1990.

[9] Ajjarapu, V. and B. Lee. "Bifurcation Theory And Its Application To Nonlinear Dynamical Phenomena In An Electrical Power System." To be presented in '91 PICA Conference and appear in IEEE Transactions on Power System.

[10] Seydel, Rüdiger. *From Equilibrium to Chaos.* New York: Springer–Verlag, 1988.

[11] *MACSYMA*: Symbolics, Inc., Burlington, MA.

[12] Hassard, B. D., N.D. Kazarinoff, and Y–H Wan. *Theory and Applications of Hopf Bifurcation. London Math. Soc. Lect. Note Series No.41.* London: Cambridge University Press, UK, 1981.

[13] Kocak, Husein. *Differential and Difference Equations through Computer Experiments.* New York: Springer–Verlag, 1989.

[14] Guckenheimer, J. and P. J. Holmes. *Nonlinear Oscillation, Dynamical systems, and Bifurcations of Vector Fields.* New York: Springer–Verlag, 1983.

[15] Arnold, V. *Geometrical Methods in the Theory of Ordinary Differential Equations.* New York: Springer–Verlag, 1983.

[16] Doedel, Eusebius. *AUTO, Software for Continuation and Bifurcation Problems in Ordinary Differential Equations.* Pasadena, Calif.: California Institute of Technology, 1986.

[17] Christy, Collin D. *Analysis of Steady State Voltage Stability in Large Scale Power System.* Master's Thesis. Iowa State University, Ames, Iowa, 1990.

[18] Rheinboldt, W. C. and J. V. Burkardt. *A Locally Parameterized Continuation Process.* ACM Transactions on Mathematical Software, 9 No. 4 (June 1983): 215-235.

[19] Wiggins, Stephen. *Introduction to Applied Nonlinear Dynamical Systems and Chaos.* New York: Springer-Verlag, 1990.

[20] Rand, Richard H. *Perturbation Methods, Bifurcation Theory, and Computer Algebra*, Applied Mathematical Sciences. Vol.65. New York: Springer-Verlag, 1987.

[21] ArrowSmith, D. K. and C. M. Place. *Ordinary Differential Equations.* New York: Chapman and Hall, 1982

APPENDIX A. A SAMPLE POWER SYSTEM MODEL

Consider the power system model shown in Figure 5.1 that was developed in reference [4]. One generator is a slack bus and the other generator has constant voltage magnitude E_m and angle dynamics given by the swing equation

$$\begin{aligned} M\ddot{\delta} = \; & -d_m\omega + P_m + E_m V Y_m \sin(\delta_L - delta - \theta_m) \\ & + E_m^2 Y_m \sin\theta_m \end{aligned} \tag{A.1}$$

where M, d_m, and P_m are the generator inertia, damping and mechanical power respectively.

The load model includes a dynamic induction motor model with a constant PQ load in parallel. The dynamic induction motor model specifies the real and reactive power demands of the motor in terms of load voltage and frequency. The combined model for the motor and the PQ load is

$$P = P_0 + P_1 + K_{p\omega}\dot{\delta}_L + K_{pv}(V + T\dot{V}) \tag{A.2}$$

$$Q = Q_0 + Q_1 + K_{q\omega}\dot{\delta}_L + K_{qv}V + K_{qv_2}V^2 \tag{A.3}$$

where P_0, Q_0 are the constant real and reactive powers of the motor and P_1, Q_1 represent the PQ load.

Q_1 is chosen as the system parameter so that increasing Q_1 corresponds to increasing the load reactive power demand. The load also includes a fixed capacitor

C to raise the voltage up to 1.0 per unit. The Thevenin equivalent of the circuit including reference bus is seen from the capacitor is given by:

$$E_0^{'} = E_0/(1 + C^2 Y_0^{-2} - 2CY_0^{-1}\cos(\theta_0))^{\frac{1}{2}} \quad (A.4)$$

$$Y_0^{'} = Y_0(1 + C^2 Y_0^{-2} - 2CY_0^{-1}\cos(\theta_0))^{\frac{1}{2}} \quad (A.5)$$

$$\theta_0^{'} = \theta_0 + \tan^{-1}\left(\frac{CY_0^{-1}\sin(\theta_0)}{1 - CY_0^{-1}\cos(\theta_0)}\right) \quad (A.6)$$

The real and reactive powers supplied to the load network are

$$\begin{aligned} P = & -E_0^{'}Y_0^{'}\sin(\delta_L + \theta_0^{'}) - \\ & E_m Y_m V \sin(\delta_L - \delta + \theta_m) \\ & +(Y_0^{'}\sin(\theta_0^{'}) + Y_m \sin(\theta_m))V^2 \end{aligned} \quad (A.7)$$

$$\begin{aligned} Q = & E_0^{'}Y_0^{'}\cos(\delta_L + \theta_0^{'}) + \\ & E_m Y_m V \cos(\delta_L - \delta + \theta_m) \\ & -(Y_0^{'}\cos(\theta_0^{'}) + Y_m \cos(\theta_m))V^2 \end{aligned} \quad (A.8)$$

Algebraic manipulation of A.1 through A.8 results in the following four dynamical equations:

$$\dot{\delta} = \omega \quad (A.9)$$

$$\begin{aligned} M\dot{\omega} = & -\delta\omega + P_m \\ & +E_m Y_m V \sin(\delta_L - \delta - \theta_m) \\ & +E_M^2 Y_m \sin(\theta_m) \end{aligned} \quad (A.10)$$

$$\begin{aligned} K_{q\omega}\dot{\delta_L} = & -K_{qv_2}V^2 - K_{qv}V \\ & +E_0^{'}Y_0^{'}V\cos(\delta_L + \theta_0^{'}) \end{aligned} \quad (A.11)$$

$$
\begin{aligned}
& + E_m Y_m V \cos(\delta_L - \delta + \theta_m) \\
& -(Y_0^{'} \cos(\theta_0^{'}) + Y_m \cos(\theta_m)) V^2 \\
& - Q_0 - Q_1 \\
T K_{q\omega} K_{pv} \dot{V} \;=\; & K_{p\omega} K_{qv_2} V^2 \\
& + (K_{p\omega} K_{qv} - K_{q\omega} K_{pv}) V \\
& \sqrt{(K_{q\omega}^2 + K_{p\omega}^2)}[-E_0^{'} Y_0^{'} V \\
& \cos(\delta_L + \theta_0^{'} - \eta) \\
& - E_m Y_m V \cos(\delta_L - \delta + \theta_m - \eta) \\
& + (Y_0^{'} \cos(\theta_0^{'} - \eta) \\
& + Y_m \cos(\theta_m - \eta)) V^2] \\
& - K_{q\omega}(P_0 + P_1) K_{p\omega}(Q_0 + Q_1)
\end{aligned}
\tag{A.12}
$$

where

$$\eta = \tan^{-1}(\frac{K_{q\omega}}{K_{p\omega}}).$$

The load parameter values are

$$
\begin{aligned}
K_{p\omega} = 0.4, \quad K_{pv} = 0.3, \quad K_{q\omega} = -0.03, \\
K_{qv} = -2.8, \quad K_{qv_2} = 2.1, \quad T = 8.5 \\
P_0 = 0.6, \quad Q_0 = 1.3, \quad P_1 = 0.0
\end{aligned}
\tag{A.13}
$$

and the network and generator parameter values are

$$
\begin{aligned}
Y_0 = 20.0, \quad \theta_0 = -5.0, \quad E_0 = 1.0, \\
C = 12.0, \quad Y_0^{'} = 8.0, \quad \theta_0^{'} = -12.0,
\end{aligned}
\tag{A.14}
$$

$$E_0' = 2.5, \quad Y_m = 5.0, \quad \theta_m = -5.0,$$

$$E_m = 1.0, \quad P_m = 1.0, \quad d_m = 0.05,$$

$$M = 0.3$$

All values are in per unit except for angles, which are in degrees.

APPENDIX B. STABILITY AT HOPF BIFURCATION POINT

Here, we show the system stability at Hopf Bifurcation point conceptually. On the center manifold the Equation 3.1 has the following form

$$\dot{y}_1 = 0y_1 - Im\lambda(p)y_2 + f_1(y_1, y_2, p) \tag{B.1}$$

$$\dot{y}_2 = Im\lambda(p)y_1 + 0y_2 + f_2(y_1, y_2, p) \tag{B.2}$$

where f_1 and f_2 are strictly nonlinear in y_1 and y_2. $\lambda(p)$ and its complex conjugate $\lambda^*(p)$ are the eigenvalues of the vector field linearized about the fixed point at the origin (Hopf bifurcation point).

To obtain the above two equations, several preliminary steps were first conducted. As discussed in Chapter 3, we first transformed the fixed point to the origin and performed a transformation of the coordinates so that the A matrix had Jordan canonical form. Because a pair of complex conjugate eigenvalue becomes purely imaginary, the stable manifolds are locally expressed as follows:

$$h_1(y_1, y_2) = a_1y_1^2 + a_2y_1y_2 + a_3y_2^2 + \cdots \tag{B.3}$$

$$h_2(y_1, y_2) = b_1y_1^2 + b_2y_1y_2 + b_3y_2^2 + \cdots \tag{B.4}$$

In general the complex conjugate eigenvalue are denoted by

$$\lambda(p) = \alpha(p) \pm i\omega(p), \tag{B.5}$$

and at Hopf bifurcation

$$\alpha(p_c) = 0, \qquad \omega(p_c) \neq 0.$$

The next step is to transform Eqs.B.1 and B.2 into normal form. The method of normal forms provides a way of finding a coordinate system in which the dynamical system takes the simplest form. This was done in [19]. Rand [20] provides a software package using MACSYMA that transforms it to normal form. The normal form was found to be

$$\dot{y}_1 = \alpha(p)y_1 - \omega(p)y_2 + (a(p)y_1 - b(p)y_2)(y_1^2 + y_2^2) + \cdots \tag{B.6}$$

$$\dot{y}_2 = \omega(p)y_1 + \alpha(p)y_2 + (b(p)y_1 + a(p)y_2)(y_1^2 + y_2^2) + \cdots \tag{B.7}$$

where $a(p)$ and $b(p)$ are real and imaginary part of $c(p)$ that is a constant depending on p [19].

B.6 and B.7 are more conveniently investigated in polar coordinates. In polar coordinates, B.6 and B.7 are given by

$$\dot{r} = \alpha(p)r + a(p)r^3 + \cdots \tag{B.8}$$

$$\dot{\theta} = \omega(p) + b(p)r^2 + \cdots \tag{B.9}$$

Since we are interested in the dynamics near $p = p_c$, we expand the coefficients $\alpha(p)$, $\omega(p)$, $a(p)$, and $b(p)$ in Eqs.B.8 and B.9. Eqs. B.8 and B.9 becomes

$$\dot{r} = \alpha'(p_c)pr + a(p_c)r^3 + \cdots \tag{B.10}$$

$$\dot{\theta} = \omega(p_c) + \omega'(p_c)p + b(p_c)r^2 + \cdots \tag{B.11}$$

where $\alpha'(p_c)$ denotes $d\alpha(p_c)/dp$ and $\omega'(p_c)$ $d\omega(p_c)/dp$. Neglecting the higher order terms in B.10 and B.11 give

$$\dot{r} = \alpha'(p_c)pr + a(p_c)r^3 \tag{B.12}$$

$$\dot{\theta} = \omega(p_C) + \omega^{'}(p_C)p + b(p_C)r^2. \tag{B.13}$$

In Eqs. B.12 and B.13, one can observe that the dynamics is dominated by r, because only r appears in the right hand side of both equations. To be precise, values of $r > 0$ and p for which $\dot{r} = 0$, but $\dot{\theta} \neq 0$, correspond to periodic orbit. Wiggins [19] gave explicit conditions to determine stability:

- asymptotically stable for $a < 0$;
- unstable for $a > 0$.

$a(p_C)$ is given explicitly in the form of second, third derivatives of B.3,B.4. [12] shows that β_2 is nothing but $2a(p_C)$.

APPENDIX C. THE ANALYSIS OF VOLTAGE VERSUS REACTIVE LOAD CURVE

This section basically explains affect of load modelling on voltage versus reactive load curve. The magnitude of the voltage at the load bus gradually decreases as the reactive power portion Q_1 of the constant load increases. The decrease in the load voltage causes a nonlinear change in reactive power consumed by the induction motor load as shown in the curve of V versus Q_{mot} in Figure C.1. Figures C.1 and C.2 do not include stability information, i.e., only the area around the turning point is taken into account. The reactive power injected into the load is the sum of the reactive powers of each load. Figure C.1 shows that increasing Q_1 corresponds to increasing the load reactive power demand Q_{tot} injected into the load bus. However, the voltage versus Q_{tot} curve has a peak, which is not the critical point. On the curve corresponding to Q_{tot}, the critical point is located at the point corresponding to V_{cr} below peak.

When a constant PQ load, which is independent of system voltage, is considered instead of induction motor, the reactive power curves of the individual load are shown in Figure C.2. The curve of total reactive power injected into the load bus has a critical point at its peak.

Usually in the region below the peak point, the system is considered unstable,

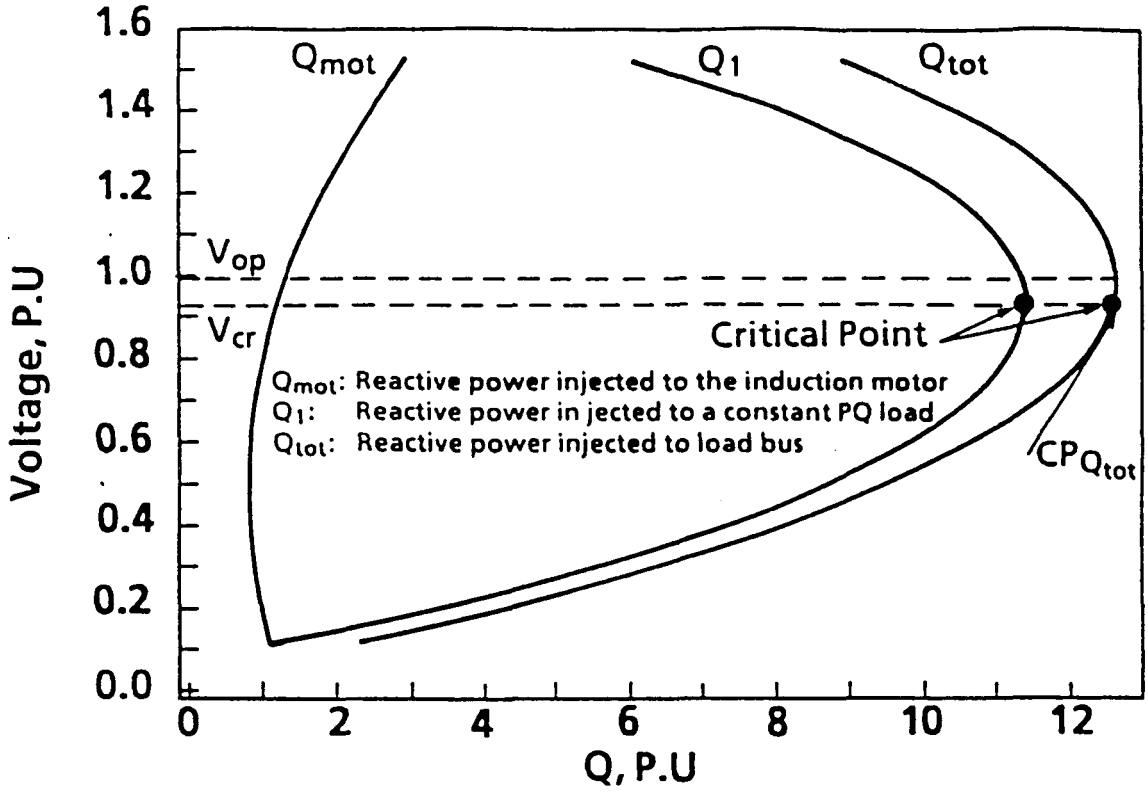

Figure C.1: Load voltage versus reactive power of constant PQ load with induction motor in parallel

but it is not always true. Figures C.1 and C.2 indicate that the induction motor moves the critical point of Q_{tot} below the peak. It may be stable depending on the characteristics of individual loads even if the system operates below the peak.

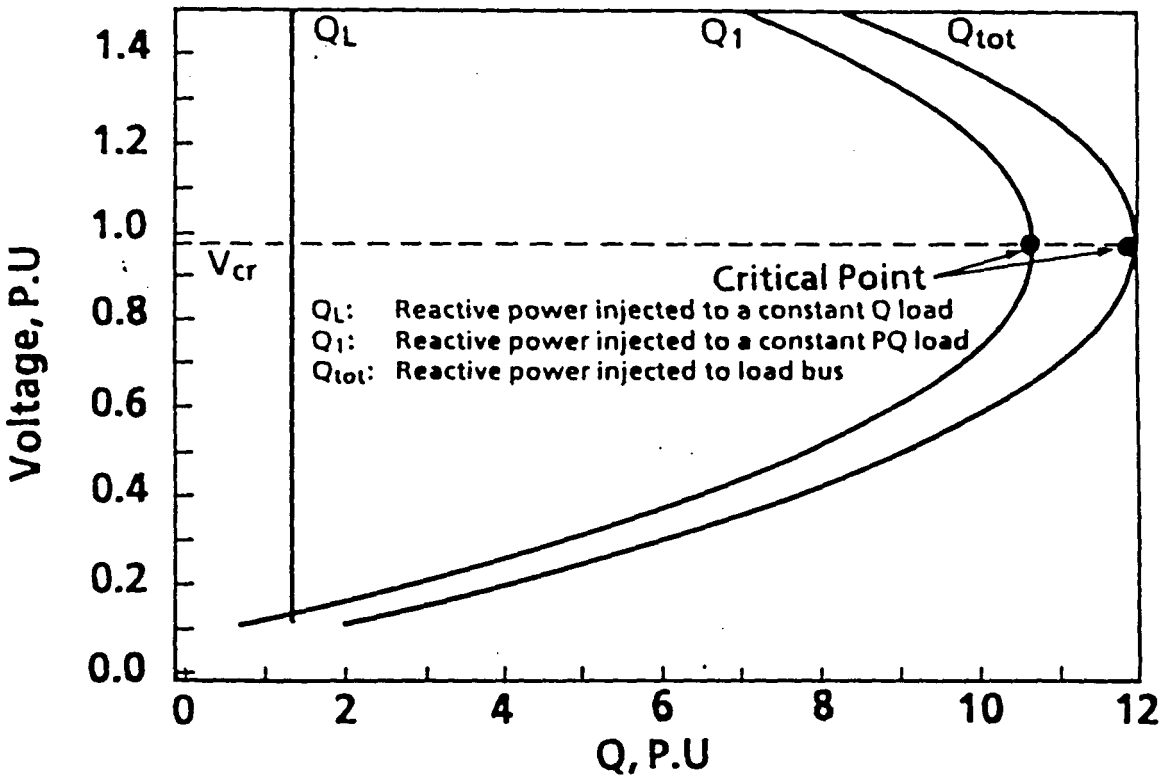

Figure C.2: Load voltage versus reactive power of constant PQ load